IEEE Access
Multidisciplinary | Rapid Review | Open Access Journal

Received June 28, 2019, accepted July 15, 2019, date of publication July 25, 2019, date of current version August 9, 2019.

Digital Object Identifier 10.1109/ACCESS.2019.2931181

A Novel Sampling Frequency Offset Estimation Algorithm for OFDM Systems Based on Cyclostationary Properties

MANISH KUMAR AND RON DABORA, (Senior Member, IEEE)
Department of Electrical and Computer Engineering, Ben-Gurion University, Be'er-Sheva 8410501, Israel

Corresponding author: Ron Dabora (ron@ee.bgu.ac.il)

This work was supported in part by the Israeli Ministry of Economy through the HERON 5G Consortium and in part by the Israel Science Foundation under Grant 1685/16.

ABSTRACT Sampling frequency synchronization in orthogonal frequency division multiplexing (OFDM) communications is critical for achieving the full advantages offered by this modulation scheme. In this paper, we propose a novel and efficient, blind, cyclostationarity-based sampling frequency synchronization (CB-SFS) algorithm for estimating the sampling frequency offset (SFO) in OFDM communications by exploiting the relationship between the sampling frequency and the cyclostationary properties of the sampled received signal. The proposed scheme is ignorant of the channel coefficients and does not require pilots. These two properties are rather unique in this context and are not possessed by previous schemes which achieve comparable estimation performance. These properties also make the proposed CB-SFS scheme suitable for a wide range of communications scenarios. The main novelty of the new scheme is the understanding that SFO alters the cycle frequencies at the receiver, yet these frequencies are a priori known for the discrete-time (DT) transmitted signal, as they result from the periodic operation of the DT signal generation scheme at the transmitter. We show that the mismatch between the measured and the expected cycle frequencies is directly related to the SFO. Complexity analysis and numerical simulations are carried out and demonstrate the superiority of the proposed CB-SFS algorithm compared to the existing approaches. It is illustrated that the proposed algorithm can achieve a smaller estimation error at the same complexity order of current algorithms while providing a higher spectral efficiency and robustness to additive stationary noise and to multipath.

INDEX TERMS Orthogonal frequency division multiplexing, sampling frequency offset, synchronization, cyclostationary processes, almost cyclostationary processes.

I. INTRODUCTION

Orthogonal frequency division multiplexing (OFDM) is a multicarrier modulation scheme which is widely used in current wireless communications standards, and is also considered a major candidate for future communications systems [1]. Two of the major advantages of OFDM modulation are its spectral efficiency and its robustness to frequency-selective fading [2]. However, these advantages are obtained only when the OFDM receiver is synchronized with the transmitter, as synchronization errors, and in particular sampling frequency offset (SFO) and carrier frequency offset (CFO) induce intercarrier interference (ICI) which substantially degrades communications performance [3]. For this reason, estimation of SFO and of CFO have been receiving significant research focus throughout the years.

Several algorithms for SFO synchronization in OFDM communications have been proposed throughout the years. These algorithms can be generally classified into two types: Data-aided (DA) algorithms, which use dedicated pilot symbols to facilitate parameter estimation, e.g., [4]–[8], and non-data-aided (also referred to as blind) algorithms, which do not use dedicated pilot symbols, e.g., [9]–[11]. As wireless spectrum is a very scarce resource, blind schemes are advantageous to DA schemes in modern wireless communications systems, due to their higher spectral efficiency.

The associate editor coordinating the review of this manuscript and approving it for publication was Khaled Rabie.

In the class of DA schemes we note the work in [4], which presents a DA SFO estimation algorithm for OFDM communications based on exploiting the phase differences between the pilot symbols. In [5], the authors propose an algorithm for SFO estimation using the channel frequency response, where pilot patterns with a maximum channel power (i.e., the magnitude-squared of the channel frequency response) are chosen to facilitate robustness of the estimate with respect to the frequency-selectivity of the channel. In [6], a DA algorithm for the joint acquisition of the SFO and the CFO for OFDM signals is proposed. The algorithm uses two long training symbols in the preamble and obtains closed-form maximum-likelihood (ML) estimates of the SFO and the CFO by exploiting the phase shift between the two training symbols in the frequency domain. The work in [7] proposes a DA algorithm for SFO estimation based on using continual pilots which occupy the same subcarrier locations in different OFDM symbols. The SFO is then estimated using the selected pilots set via a least-squares estimation (LSE). The work in [8] proposes a DA ML scheme for estimating the SFO which exploits the Toeplitz structure of the covariance matrix of the time-domain observations to reduce the computational complexity of the estimator.

In the class of blind schemes we note the work [9] which proposes a blind frequency synchronization algorithm which uses oversampling to fully exploit the phase shift among neighboring samples, leading to a root-finding problem that allows for a computationally efficient estimation. In [10], a blind estimation algorithm is proposed which estimates the SFO using the phase difference between the outputs of two different fast Fourier transforms (FFTs) windows taken within an OFDM symbol duration. This blind estimator is stated in a closed form, thereby avoiding the computational complexity of a grid search, which is common in SFO estimation algorithms. Lastly, in [11] a blind SFO estimation algorithm over frequency-selective fading channels is proposed, which uses the second order statistics of the received OFDM signal.

The fact that using pilots to facilitate synchronization reduces the spectral efficiency of the communications link, motivated the present work in which we introduce a novel, efficient cyclostationarity-based sampling frequency synchronization (CB-SFS) algorithm, which exploits the cyclostationarity of the received signal *without* using a dedicated pilot sequence, while requiring a reasonable complexity as compared to the previously proposed algorithms. The novelty of the proposed algorithm follows as it does not estimate the sampling frequency directly, but instead it adjusts the cycle frequencies of the sampled received signal, estimated via [12], [13], to align with those of the transmitted signal. Note that the cycle frequencies of the transmitted signal are completely determined by the signal generation scheme, hence are available at the receiver. The performance of the proposed CB-SFS algorithm is evaluated and compared with the major alternative approaches via an extensive numerical study. It is shown that the CB-SFS algorithm achieves smaller estimation errors with the same complexity order and with a higher spectral efficiency compared to previously proposed algorithms. The new algorithm is also robust to the actual channel coefficients and to symbol timing offset (STO) synchronization.

The rest of this paper is organized as follows: Section II presents a brief review of wide-sense cyclostationary (WSCS) and of wide-sense almost-cyclostationary (WSACS) random processes. Section III presents the system model. Section IV provides a stochastic characterization of the discrete-time (DT) received signal obtained by sampling the continuous-time (CT) received signal. Section V presents the proposed CB-SFS algorithm, along with its complexity analysis. The numerical analysis and discussions are presented in the Section VI, followed by the concluding remarks in the Section VII.

Notations: In the following, complex conjugate, stochastic expectation, and the convolution operator are represented by $(\cdot)^*$, $\mathbb{E}\{\cdot\}$, and $\star$, respectively. The sets of integers, positive integers, rational numbers, real numbers and complex numbers are denoted by $\mathcal{Z}$, $\mathcal{N}$, $\mathcal{Q}$, $\mathcal{R}$, and $\mathcal{C}$ respectively. $\Re\{z\}$ and $\Im\{z\}$ denote the real and the imaginary parts of $z \in \mathcal{C}$. For a set $\mathcal{A}$, we use $|\mathcal{A}|$ to denote its cardinality. Lastly, CT random processes are denoted using capital letters and round brackets, e.g., $X(t)$, where $t \in \mathcal{R}$ denotes the time. Similarly, DT random processes are denoted using capital letters and square brackets, e.g., $X[n]$, where $n \in \mathcal{Z}$ is the DT index.

II. CYCLOSTATIONARY AND ALMOST-CYCLOSTATIONARY RANDOM PROCESSES

We first recall the definition of a WSCS random process from [14, Sec. 3.2]:

Definition 1*: A proper complex CT (resp. DT) random process $X(t)$ (resp. $X[n]$) is said to be WSCS if both its mean and its autocorrelation function (AF), are periodic with some period T_0 (resp. N_0) for any lag value $\tau \in \mathcal{R}$ (resp. $\Delta \in \mathcal{Z}$).*

From the above definition, it follows that for the WSCS random process $X(t)$ (resp. $X[n]$), the mean $m_X(t)$ (resp. $m_X[n]$) and the AF $\mathcal{R}_X(t,\tau)$ (resp. $\mathcal{R}_X[n,\Delta]$) can be represented as

$$\mathbb{E}\{X(t)\} \triangleq m_X(t) = m_X(t+T_0) \tag{1a}$$
$$\mathbb{E}\{X(t)X^*(t-\tau)\} \triangleq \mathcal{R}_X(t,\tau) = \mathcal{R}_X(t+T_0,\tau), \tag{1b}$$

$$\mathbb{E}\{X[n]\} \triangleq m_X[n] = m_X[n+N_0] \tag{2a}$$
$$\mathbb{E}\{X[n]X^*[n-\Delta]\} \triangleq \mathcal{R}_X[n,\Delta] = \mathcal{R}_X[n+N_0,\Delta]. \tag{2b}$$

Since for a CT WSCS process $X(t)$, the AF $\mathcal{R}_X(t,\tau)$ is periodically varying in the time variable t, it can be expanded into a Fourier series in t, see [14, Eqn. (3.61)]:

$$\mathcal{R}_X(t,\tau) = \sum_{k=-\infty}^{\infty} \mathcal{R}_X^{k/T_0}(\tau) e^{j2\pi \frac{k}{T_0} t},$$

where the coefficients $\mathcal{R}_X^{k/T_0}(\tau)$ are referred to as the cyclic autocorrelation function (CAF), $\frac{k}{T_0}$, where $k \in \mathcal{Z}$, is referred

to as the cycle frequency, and τ is the lag variable. The CAF $\mathcal{R}_X^{k/T_0}(\tau)$ is obtained using [14, Eqn. (3.63)]:

$$\mathcal{R}_X^{k/T_0}(\tau) = \frac{1}{T_0}\int_{t=-T_0/2}^{T_0/2} \mathcal{R}_X(t,\tau)e^{-j2\pi\frac{k}{T_0}t}dt. \tag{3}$$

Similarly, for the DT WSCS process $X[n]$, the AF $\mathcal{R}_X[n,\Delta]$ can be expanded into a Fourier series as [14, Eqn. (3.108)]:

$$\mathcal{R}_X[n,\Delta] = \sum_{k\in\mathcal{N}_0} \mathcal{R}_X^{\alpha_k}[\Delta]e^{j2\pi\alpha_k n}, \tag{4}$$

where $\alpha_k \equiv \frac{k}{N_0}$, $k \in \mathcal{N}_0 \triangleq \{0,1,\ldots,N_0-1\}$ are the cycle frequencies. The CAF $\mathcal{R}_X^{\alpha_k}[\Delta]$ for the process $X[n]$ can be obtained using [14, Eqn. (3.109)]:

$$\mathcal{R}_X^{\alpha_k}[\Delta] = \frac{1}{N_0}\sum_{n=0}^{N_0-1} \mathcal{R}_X[n,\Delta]e^{-j2\pi\alpha_k n}. \tag{5}$$

We next recall the definition of a WSACS random process, see also [14, Sec. 3.2]:

Definition 2: A proper complex CT (resp. DT) random process $S(t)$ (resp. $S[n]$) is said to be WSACS if both its mean and its AF are almost-periodic functions[1] *in the time variable t (resp. DT index n).*

From the above definition, it follows that for the CT WSACS random process $S(t)$, the mean $\mathbb{E}\{S(t)\}$ and the AF $\mathcal{R}_S(t,\tau) = \mathbb{E}\{S(t)S^*(t-\tau)\}$ can be represented as [14, Eqns. (3.10), (3.73)]:

$$\mathbb{E}\{S(t)\} = \sum_{\alpha\in\mathcal{A}} \mu_S^\alpha e^{j2\pi\alpha t}\ ;\ \mathcal{R}_S(t,\tau) = \sum_{\alpha\in\mathcal{A}} \mathcal{R}_S^\alpha(\tau)e^{j2\pi\alpha t} \tag{6}$$

where $\mathcal{A}$ is a countable set of cycle frequencies which are possibly incommensurate. The CAF $\mathcal{R}_S^\alpha(\tau)$ for $S(t)$ is obtained as the limit [14, Eqns. (3.11), (3.74)]:

$$\mathcal{R}_S^\alpha(\tau) = \lim_{T\to\infty}\frac{1}{T}\int_{t=-T/2}^{T/2} \mathcal{R}_S(t,\tau)e^{-j2\pi\alpha t}dt. \tag{7}$$

Similarly, for the DT random process $S[n]$, the mean $\mathbb{E}\{S[n]\}$ and the AF $\mathcal{R}_S[n,\Delta] = \mathbb{E}\{S[n]S^*[n-\Delta]\}$ can be represented as [14, Eqn. (3.30)], [16, Eqn. (4.20)]:

$$\mathbb{E}\{S[n]\} = \sum_{\tilde{\alpha}\in\tilde{\mathcal{A}}} \mu_S^{\tilde{\alpha}} e^{j2\pi\tilde{\alpha}n}\ ;\ \mathcal{R}_S[n,\Delta] = \sum_{\tilde{\alpha}\in\tilde{\mathcal{A}}} \mathcal{R}_S^{\tilde{\alpha}}[\Delta]e^{j2\pi\tilde{\alpha}n} \tag{8}$$

with $\tilde{\mathcal{A}}$ being a countable set of cycle frequencies which are possibly incommensurate. The CAF $\mathcal{R}_S^{\tilde{\alpha}}[\Delta]$ of $S[n]$ is obtained as the limit [14, Eqn. (3.31)], [16, Eqn. (4.21)]

$$\mathcal{R}_S^{\tilde{\alpha}}[\Delta] = \lim_{N\to\infty}\frac{1}{2N+1}\sum_{n=-N}^{N} \mathcal{R}_S[n,\Delta]e^{-j2\pi\tilde{\alpha}n}. \tag{9}$$

[1] See [15, Ch. I] for the definition of an almost-periodic function.

III. SYSTEM MODEL

Let N_{sc} denote the number of subcarriers in an OFDM symbol and $D_{m,k}$ denote the complex random data symbols at the k-th subcarrier of the m-th OFDM symbol in the sequence, $k \in [0, N_{\text{sc}}-1]$ and $m \in \mathcal{Z}$. We assume that each data symbol $D_{m,k}$ is selected uniformly from a finite, zero-mean and proper complex set of constellation points $\mathcal{D}$ in an independent and identically distributed (i.i.d.) manner over k and m. Thus,

$$\mathbb{E}\{D_{m,k}D^*_{\tilde{m},\tilde{k}}\} = \sigma_D^2\cdot\delta[m-\tilde{m}]\cdot\delta[k-\tilde{k}] \tag{10a}$$

$$\mathbb{E}\{D_{m,k}\} = 0,\ \mathbb{E}\{D_{m,k}D_{\tilde{m},\tilde{k}}\} = 0. \tag{10b}$$

The modulated DT sequence for the m-th OFDM symbol is obtained from $D_{m,k}$ by applying an inverse discrete Fourier transform (IDFT) of size N_{sc} and then concatenating a cyclic prefix (CP) of length N_{cp} samples to the IDFT output sequence. It follows that the length of the resulting OFDM symbol in time samples is $N_{\text{sym}} = N_{\text{sc}} + N_{\text{cp}}$. Letting $T_{\text{samp}}^{(\text{sync})}$ be the sampling interval at the transmitter, we also define $T_{\text{sc}} \triangleq N_{\text{sc}}\cdot T_{\text{samp}}^{(\text{sync})}$, $T_{\text{cp}} \triangleq N_{\text{cp}}\cdot T_{\text{samp}}^{(\text{sync})}$, and $T_{\text{sym}} = T_{\text{sc}} + T_{\text{cp}}$. The transmitted complex baseband OFDM signal $S(t)$ can be represented as in [17, Eqns. (1)-(2)] (the reference time for the phase is set to the start of each symbol, see, e.g., [18, Eqn. (1)]):

$$S(t) = \frac{1}{\sqrt{T_{\text{sc}}}}\sum_{m=-\infty}^{\infty}\sum_{k=0}^{N_{\text{sc}}-1} D_{m,k}\, e^{j\frac{2\pi}{T_{\text{sc}}}k(t-mT_{\text{sym}})}p(t-mT_{\text{sym}}) \tag{11}$$

where the real-valued pulse shaping function $p(t)$ satisfies $p(t) = 1$ for $0 \le t < T_{\text{sym}}$ and $p(t) = 0$ otherwise. Letting f_{Tx} and ϕ_{Tx} denote the carrier frequency and phase, respectively, at the transmitter, the transmitted real passband signal corresponding to the baseband signal $S(t)$ is given as

$$S_{\text{pass}}(t) = \Re\left\{S(t)e^{j(2\pi f_{\text{Tx}}t+\phi_{\text{Tx}})}\right\}. \tag{12}$$

In this work, we consider a block fading passband channel whose coherence time is on the order of the frame duration, which can be modeled as a causal linear time-invariant system [17], [19]. Letting $h(t)$ denote the channel impulse response (CIR) and $W_{\text{pass}}(t)$ denote the passband additive white Gaussian noise (AWGN) at the receiver, the received passband signal $R(t)$ can be represented as $R_{\text{pass}}(t) = S_{\text{pass}}(t)\star h(t) + W_{\text{pass}}(t)$, leading to the following expression

$$\begin{aligned} R_{\text{pass}}(t) &= \int_{\lambda=0}^{\infty} h(\lambda)S_{\text{pass}}(t-\lambda)d\lambda + W_{\text{pass}}(t) \\ &= \Re\left\{\frac{1}{\sqrt{T_{\text{sc}}}}e^{j(2\pi f_{\text{Tx}}t+\phi_{\text{Tx}})}\sum_{m=-\infty}^{\infty}\sum_{k=0}^{N_{\text{sc}}-1} D_{m,k}\int_{\lambda=0}^{\infty} h(\lambda)\right. \\ &\quad \left.\cdot\, e^{-j2\pi f_{\text{Tx}}\lambda}e^{j\frac{2\pi}{T_{\text{sc}}}k(t-\lambda-mT_{\text{sym}})}p(t-\lambda-mT_{\text{sym}})d\lambda\right\} \\ &\quad + W_{\text{pass}}(t). \end{aligned} \tag{13}$$

The receiver uses an oscillator with frequency f_{Rx} and phase ϕ_{Rx} to downconvert the received passband signal to a baseband signal $R(t)$. Using the identity $\Re\{\theta\} = (\theta + \theta^*)/2$, and denoting $\Delta_{\mathrm{f}} = f_{\mathrm{Tx}} - f_{\mathrm{Rx}}$, $\Delta_\phi = \phi_{\mathrm{Tx}} - \phi_{\mathrm{Rx}}$, $\Sigma_{\mathrm{f}} = f_{\mathrm{Tx}} + f_{\mathrm{Rx}}$, and $\Sigma_\phi = \phi_{\mathrm{Tx}} + \phi_{\mathrm{Rx}}$, the downconverted baseband signal can be written as

$$\begin{aligned} R(t) &= R_{\mathrm{pass}}(t) \cdot e^{-j(2\pi f_{\mathrm{Rx}} t + \phi_{\mathrm{Rx}})} \\ &= \frac{1}{2\sqrt{T_{\mathrm{sc}}}} \sum_{m=-\infty}^{\infty} \sum_{k=0}^{N_{\mathrm{sc}}-1} \Bigg[e^{j(2\pi \Delta_{\mathrm{f}} t + \Delta_\phi)} D_{m,k} \int_{\lambda=0}^{\infty} h(\lambda) \\ &\quad \cdot e^{-j2\pi f_{\mathrm{Tx}} \lambda} e^{j\frac{2\pi}{T_{\mathrm{sc}}} k(t-\lambda-mT_{\mathrm{sym}})} p(t-\lambda-mT_{\mathrm{sym}}) d\lambda \\ &\quad + e^{-j(2\pi \Sigma_f t + \Sigma_\phi)} D_{m,k}^* \int_{\lambda=0}^{\infty} h(\lambda) e^{j2\pi f_{\mathrm{Tx}} \lambda} \\ &\quad \cdot e^{-j\frac{2\pi}{T_{\mathrm{sc}}} k(t-\lambda-mT_{\mathrm{sym}})} p(t-\lambda-mT_{\mathrm{sym}}) d\lambda \Bigg] \\ &\quad + W_{\mathrm{pass}}(t) \cdot e^{-j(2\pi f_{\mathrm{Rx}} t + \phi_{\mathrm{Rx}})}. \end{aligned} \tag{14}$$

The receive filter is a causal band-limited low-pass filter (LPF) which keeps only the received baseband signal component. Letting $W(t)$ denote the circularly symmetric complex normal noise process at the output of the receive LPF, the output signal of the receive LPF can be expressed as

$$\begin{aligned} Y(t) &= \frac{1}{2\sqrt{T_{\mathrm{sc}}}} e^{j2\pi \Delta_{\mathrm{f}} t} e^{j\Delta_\phi} \sum_{m=-\infty}^{\infty} \sum_{k=0}^{N_{\mathrm{sc}}-1} D_{m,k} \int_{\lambda=0}^{\infty} h(\lambda) \\ &\quad \cdot e^{-j2\pi f_{\mathrm{Tx}} \lambda} e^{j\frac{2\pi}{T_{\mathrm{sc}}} k(t-\lambda-mT_{\mathrm{sym}})} p(t-\lambda-mT_{\mathrm{sym}}) d\lambda \\ &\quad + W(t). \end{aligned} \tag{15}$$

The signal path model from the transmitter to the receiver is schematically depicted in Fig. 1.

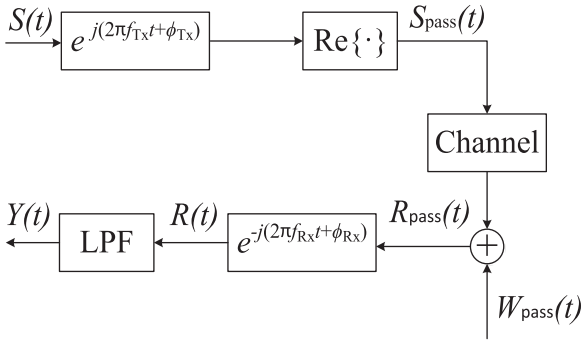

FIGURE 1. A schematic description of the signal path model.

IV. STATISTICS OF THE CT SIGNALS AND OF THE SAMPLED RECEIVED SIGNAL

In this section we establish the cyclostationarity of the CT transmitted and received signals along the signal path, and subsequently we consider the statistics of the sampled received signal.

A. CYCLOSTATIONARITY OF $S(t)$, $R(t)$, and $Y(t)$

From (10)-(11), the first-order statistics of $S(t)$ is

$$\begin{aligned} m_S(t) &\triangleq \mathbb{E}\{S(t)\} \\ &= \frac{1}{\sqrt{T_{\mathrm{sc}}}} \sum_{m=-\infty}^{\infty} \sum_{k=0}^{N_{\mathrm{sc}}-1} \mathbb{E}\{D_{m,k}\} e^{j\frac{2\pi}{T_{\mathrm{sc}}} k(t-mT_{\mathrm{sym}})} \\ &\quad \cdot p(t-mT_{\mathrm{sym}}) \\ &= 0 \\ &= m_S(t+T_{\mathrm{sym}}). \end{aligned} \tag{16}$$

Next, the AF of $S(t)$, denoted, $\mathcal{R}_S(t,\tau) \triangleq \mathbb{E}\{S(t)S^*(t-\tau)\}$ can be expressed as:

$$\begin{aligned} \mathcal{R}_S(t,\tau) &= \frac{1}{T_{\mathrm{sc}}} \sigma_D^2 \sum_{k=0}^{N_{\mathrm{sc}}-1} e^{j2\pi \frac{k}{T_{\mathrm{sc}}} \tau} \sum_{m=-\infty}^{\infty} p(t-mT_{\mathrm{sym}}) \\ &\quad \cdot p(t-\tau-mT_{\mathrm{sym}}) \\ &\overset{(a)}{=} \frac{1}{T_{\mathrm{sc}}} \sigma_D^2 \sum_{k=0}^{N_{\mathrm{sc}}-1} e^{j2\pi \frac{k}{T_{\mathrm{sc}}} \tau} \sum_{\underline{m}=-\infty}^{\infty} p(t-\underline{m}T_{\mathrm{sym}}) \\ &\quad \cdot p(t-\tau-\underline{m}T_{\mathrm{sym}}) \\ &= \mathcal{R}_S(t+T_{\mathrm{sym}},\tau), \end{aligned} \tag{17}$$

where in step (a) we set $\underline{m} = (m-1)$. It follows from (16)-(17) that $m_S(t) = m_S(t+T_{\mathrm{sym}})$ and $\mathcal{R}_S(t,\tau) = \mathcal{R}_S(t+T_{\mathrm{sym}},\tau)$, and thus, the transmitted baseband signal $S(t)$ is WSCS with period T_{sym} for a sufficiently long sequence of OFDM symbols. Note that strictly speaking, (16)-(17) hold when m varies over the entire set $\mathcal{Z}$, thus for a finite number of OFDM symbols, $S(t)$ can be well approximated as a WSCS process when the number of OFDM symbols is sufficiently large. Next, using (10) and (14), it directly follows that the first-order statistics of $R(t)$ satisfies

$$m_R(t) \triangleq \mathbb{E}\{R(t)\} = 0 = m_R(t+T_{\mathrm{sym}}). \tag{18}$$

In Appendix A, the second-order statistics of $R(t)$, denoted $\mathcal{R}_R(t,\tau)$ is derived using (10) and (14), and is shown to satisfy $\mathcal{R}_R(t,\tau) = \mathcal{R}_R(t+T_{\mathrm{sym}},\tau)$. It therefore follows that $R(t)$ is WSCS with period T_{sym} for a sufficiently long sequence of OFDM symbols.

Lastly, we consider the statistics of the CT received signal $Y(t)$. Using (10) and (15), we obtain that the first-order statistics of $Y(t)$ satisfies

$$m_Y(t) \triangleq \mathbb{E}\{Y(t)\} = 0 = m_Y(t+T_{\mathrm{sym}}), \tag{19}$$

and derive the AF of $Y(t)$ as

$$\begin{aligned} \mathcal{R}_Y(t,\tau) &\triangleq \mathbb{E}\{Y(t)Y^*(t-\tau)\} \\ &= \frac{1}{4T_{\mathrm{sc}}} \sigma_D^2 e^{j2\pi \Delta_{\mathrm{f}} \tau} \sum_{m=-\infty}^{\infty} \sum_{k=0}^{N_{\mathrm{sc}}-1} e^{j2\pi \frac{k}{T_{\mathrm{sc}}} \tau} \\ &\quad \cdot \int_{\lambda=0}^{\infty} h(\lambda) e^{-j2\pi \left(f_{\mathrm{Tx}} + \frac{k}{T_{\mathrm{sc}}}\right)\lambda} p(t-\lambda-mT_{\mathrm{sym}}) d\lambda \end{aligned}$$

$$\cdot \int_{\tilde{\lambda}=0}^{\infty} h(\tilde{\lambda}) e^{j2\pi\left(f_{\mathrm{Tx}}+\frac{k}{T_{\mathrm{sc}}}\right)\tilde{\lambda}} p(t-\tau-\tilde{\lambda}-mT_{\mathrm{sym}})d\tilde{\lambda} + \mathcal{R}_W(\tau)$$
$$= \mathcal{R}_Y(t+T_{\mathrm{sym}},\tau), \tag{20}$$

where $\mathcal{R}_W(\tau) \triangleq \mathbb{E}\{W(t)W^*(t-\tau)\}$. It follows from (19)-(20) that the received baseband signal $Y(t)$ is WSCS with period T_{sym} for a sufficiently long sequence of OFDM symbols.

B. STATISTICS OF THE SAMPLED RECEIVED SIGNAL

In order to apply digital processing, the receiver first samples $Y(t)$. In the following we analyze the relationship between the sampling interval and the statistics of the resulting DT signal.

1) SYNCHRONOUS SAMPLING OF $Y(t)$

First consider the case in which the sampling interval T_{samp} is commensurate with the symbol period T_{sym}, namely

$$\frac{T_{\mathrm{sym}}}{T_{\mathrm{samp}}} = \frac{U}{V} \tag{21}$$

where, $U, V \in \mathcal{N}$ have no common factors [20, Sec. 3]. We refer to this situation as *synchronous sampling*. The resulting DT signal, denoted $Y_{\mathrm{DT}}[n]$, is expressed as:

$$\begin{aligned} Y_{\mathrm{DT}}[n] &\triangleq Y(n\cdot T_{\mathrm{samp}}) \\ &= \frac{1}{2\sqrt{T_{\mathrm{sc}}}} e^{j(2\pi\Delta_{\mathrm{f}} nT_{\mathrm{samp}}+\Delta_\phi)} \sum_{m=-\infty}^{\infty}\sum_{k=0}^{N_{\mathrm{sc}}-1} D_{m,k} \\ &\quad \cdot \int_{\lambda=0}^{\infty} h(\lambda) e^{-j2\pi\left(f_{\mathrm{Tx}}+\frac{k}{T_{\mathrm{sc}}}\right)\lambda} e^{j\frac{2\pi}{T_{\mathrm{sc}}}k\left(n-m\frac{U}{V}\right)T_{\mathrm{samp}}} \\ &\quad \cdot p\left(\left(n-m\frac{U}{V}\right)T_{\mathrm{samp}}-\lambda\right)d\lambda + W(n\cdot T_{\mathrm{samp}}) \end{aligned} \tag{22}$$

From the statistics of $D_{m,k}$ in Eqn. (10) and from (22), we obtain that $m_{Y_{\mathrm{DT}}}[n] \triangleq \mathbb{E}\{Y_{\mathrm{DT}}[n]\} = 0$, and that the AF of $Y_{\mathrm{DT}}[n]$ is expressed as:

$$\begin{aligned} &\mathcal{R}_{Y_{\mathrm{DT}}}[n,\Delta] \\ &\triangleq \mathbb{E}\{Y_{\mathrm{DT}}[n]Y^*_{\mathrm{DT}}[n-\Delta]\} \\ &= \frac{1}{4\,T_{\mathrm{sc}}}\sigma_D^2 \sum_{m=-\infty}^{\infty}\sum_{k=0}^{N_{\mathrm{sc}}-1} e^{j2\pi\left(\Delta_{\mathrm{f}}+\frac{k}{T_{\mathrm{sc}}}\right)\Delta\cdot T_{\mathrm{samp}}} \\ &\quad \cdot \int_{\lambda=0}^{\infty} h(\lambda) e^{-j2\pi\left(f_{\mathrm{Tx}}+\frac{k}{T_{\mathrm{sc}}}\right)\lambda} p\left(\left(n-m\frac{U}{V}\right)T_{\mathrm{samp}}-\lambda\right)d\lambda \\ &\quad \cdot \int_{\tilde{\lambda}=0}^{\infty} h(\tilde{\lambda}) e^{j2\pi\left(f_{\mathrm{Tx}}+\frac{k}{T_{\mathrm{sc}}}\right)\tilde{\lambda}} p\left(\left(n-\Delta-m\frac{U}{V}\right)T_{\mathrm{samp}}-\tilde{\lambda}\right)d\tilde{\lambda} \\ &\quad +\mathcal{R}_W[\Delta] \\ &\overset{(b)}{=} \frac{1}{4\,T_{\mathrm{sc}}}\sigma_D^2 \sum_{\underline{m}=-\infty}^{\infty}\sum_{k=0}^{N_{\mathrm{sc}}-1} e^{j2\pi\left(\Delta_{\mathrm{f}}+\frac{k}{T_{\mathrm{sc}}}\right)\Delta\cdot T_{\mathrm{samp}}} \\ &\quad \cdot \int_{\lambda=0}^{\infty} h(\lambda) e^{-j2\pi\left(f_{\mathrm{Tx}}+\frac{k}{T_{\mathrm{sc}}}\right)\lambda} p\left(\left(n-\underline{m}\frac{U}{V}\right)T_{\mathrm{samp}}-\lambda\right)d\lambda \\ &\quad \cdot \int_{\tilde{\lambda}=0}^{\infty} h(\tilde{\lambda}) e^{j2\pi\left(f_{\mathrm{Tx}}+\frac{k}{T_{\mathrm{sc}}}\right)\tilde{\lambda}} p\left(\left(n-\Delta-\underline{m}\frac{U}{V}\right)T_{\mathrm{samp}}-\tilde{\lambda}\right)d\tilde{\lambda} \\ &\quad +\mathcal{R}_W[\Delta] \\ &= \mathcal{R}_{Y_{\mathrm{DT}}}[n+U,\Delta] \end{aligned} \tag{23}$$

where $\mathcal{R}_W[\Delta] \triangleq \mathbb{E}\{W[n]W^*[n-\Delta]\}$, $W[n] \triangleq W(n\cdot T_{\mathrm{samp}})$, and in step (b) we set $\underline{m} = (m-V)$. Combined with $m_{Y_{\mathrm{DT}}}[n] = 0$, we obtain that $Y_{\mathrm{DT}}[n]$ obtained through synchronously sampling $Y(t)$, is a DT WSCS process. Note that if $T_{\mathrm{samp}} = T_{\mathrm{samp}}^{(\mathrm{sync})}$ then it follows from (21) that $U = N_{\mathrm{sym}}$ and $V = 1$.

2) ASYNCHRONOUS SAMPLING OF $Y(t)$

Next, consider the case in which the sampling interval T_{samp} is incommensurate with the symbol period, see also [21, Sec. II-B], namely,

$$\frac{T_{\mathrm{sym}}}{T_{\mathrm{samp}}} = \frac{U}{V} + \xi; \qquad \xi \notin \mathcal{Q}, \quad \xi \in (0,1). \tag{24}$$

This situation is referred to as *asynchronous sampling*. For $Y_{\mathrm{DT}}[n]$ obtained with asynchronous sampling we can write

$$\begin{aligned} &Y_{\mathrm{DT}}[n] \\ &\triangleq Y(n\cdot T_{\mathrm{samp}}) \\ &= \frac{1}{2\sqrt{T_{\mathrm{sc}}}} e^{j(2\pi\Delta_{\mathrm{f}} nT_{\mathrm{samp}}+\Delta_\phi)} \sum_{m=-\infty}^{\infty}\sum_{k=0}^{N_{\mathrm{sc}}-1} D_{m,k} \\ &\quad \cdot \int_{\lambda=0}^{\infty} h(\lambda) e^{-j2\pi\left(f_{\mathrm{Tx}}+\frac{k}{T_{\mathrm{sc}}}\right)\lambda} e^{j\frac{2\pi}{T_{\mathrm{sc}}}k\left(n-m\left(\frac{U}{V}+\xi\right)\right)T_{\mathrm{samp}}} \\ &\quad \cdot p\left(\left(n-m\left(\frac{U}{V}+\xi\right)\right)T_{\mathrm{samp}}-\lambda\right)d\lambda + W(n\cdot T_{\mathrm{samp}}) \end{aligned} \tag{25}$$

Using the statistics of $D_{m,k}$, given in (10), and the expression (25), we evaluate the mean of $Y_{\mathrm{DT}}[n]$ as $m_{Y_{\mathrm{DT}}}[n] \triangleq \mathbb{E}\{Y_{\mathrm{DT}}[n]\} = 0$, and the AF of $Y_{\mathrm{DT}}[n]$, $\mathcal{R}_{Y_{\mathrm{DT}}}[n,\Delta] \triangleq \mathbb{E}\{Y_{\mathrm{DT}}[n]Y^*_{\mathrm{DT}}[n-\Delta]\}$ as:

$$\begin{aligned} &\mathcal{R}_{Y_{\mathrm{DT}}}[n,\Delta] \\ &= \frac{1}{4\,T_{\mathrm{sc}}}\sigma_D^2 \sum_{m=-\infty}^{\infty}\sum_{k=0}^{N_{\mathrm{sc}}-1} e^{j2\pi\left(\Delta_{\mathrm{f}}+\frac{k}{T_{\mathrm{sc}}}\right)\Delta\cdot T_{\mathrm{samp}}} \int_{\lambda=0}^{\infty} h(\lambda) \\ &\quad \cdot e^{-j2\pi\left(f_{\mathrm{Tx}}+\frac{k}{T_{\mathrm{sc}}}\right)\lambda} p\left(\left(n-m\left(\frac{U}{V}+\xi\right)\right)T_{\mathrm{samp}}-\lambda\right) \\ &\quad d\lambda \int_{\tilde{\lambda}=0}^{\infty} h(\tilde{\lambda}) \\ &\quad \cdot e^{j2\pi\left(f_{\mathrm{Tx}}+\frac{k}{T_{\mathrm{sc}}}\right)\tilde{\lambda}} p\left(\left(n-\Delta-m\left(\frac{U}{V}+\xi\right)\right)T_{\mathrm{samp}}-\tilde{\lambda}\right)d\tilde{\lambda} \\ &\quad +\mathcal{R}_W[\Delta] \\ &\neq \mathcal{R}_{Y_{\mathrm{DT}}}[n+\tilde{U},\Delta], \quad \forall \tilde{U} \in \mathcal{N} \end{aligned} \tag{26}$$

Comparing (26) with (23), it is observed that $\xi \notin \mathcal{Q}$ implies that the AF of $Y_{\mathrm{DT}}[n]$ is an almost-periodic function of time, and combined with $m_{Y_{\mathrm{DT}}}[n] = 0$, we obtain that $Y_{\mathrm{DT}}[n]$, generated using asynchronous sampling, is a DT WSACS process.

V. CB-SFS: AN EFFICIENT SAMPLING FREQUENCY SYNCHRONIZATION ALGORITHM

In [18] it is shown that a DT OFDM signal obtained via sampling at intervals of $T_{\text{samp}}^{(\text{sync})}$, exhibits cyclostationarity with a period of N_{sym}. Accordingly, the cycle frequencies for such a DT OFDM signal are $\alpha_k \triangleq \frac{k}{N_{\text{sym}}} = k \cdot \alpha_1$; $k = 0, 1, \cdots, N_{\text{sym}} - 1$, where $\alpha_1 = \frac{1}{N_{\text{sym}}}$ is referred to as the *fundamental cycle frequency*. Let $\mathcal{N}_\Delta$ denote the set of lags $\Delta \in \mathcal{Z}$ for which $\exists n \in \mathcal{Z}$ such that $\mathcal{R}_{Y_{\text{DT}}}[n, \Delta] \neq 0$, and let $\mathcal{A}_{\text{wscs}}$ denote the set of cycle frequencies for $Y_{\text{DT}}[n]$. As the additive noise $W[n]$ is stationary, it follows that $\mathcal{R}_W^{\alpha_k}[\Delta] = 0$, $\forall \alpha_k \neq 0$, [18, Sec. II].

In the proposed CB-SFS algorithm we use the cycle frequencies estimation algorithm proposed in [12, Sec. III], [13], which is based on the autocorrelated CAF. In the following, we briefly review this algorithm: The CAF corresponding to the sampled signal $Y_{\text{DT}}[n]$ can be estimated as [12, Eqns. (3), (4)]:

$$\mathcal{R}_{Y_{\text{DT}}}^{\alpha}[\Delta] = \lim_{L\to\infty} \frac{1}{2L+1} \sum_{n=-L}^{L} Y_{\text{DT}}[n] \cdot Y_{\text{DT}}^{*}[n-\Delta] e^{-j2\pi\alpha n}$$

for each $\Delta \in \mathcal{N}_\Delta$. Consider a segment of $Y_{\text{DT}}[n]$ whose length, denoted with N_{seg}, satisfies $N_{\text{seg}} > \max_{\Delta\in\mathcal{N}_\Delta} |\Delta|$. The segmented CAF of $Y_{\text{DT}}[n]$ can now be expressed as [12, Eqn. (12)], [13, Eqn. (12)]:

$$\mathcal{R}_{Y_{\text{DT}}}^{\alpha}[n, \Delta]_{N_{\text{seg}}} = \frac{1}{N_{\text{seg}}} \sum_{k=n}^{n+N_{\text{seg}}-1} Y_{\text{DT}}[k] \cdot Y_{\text{DT}}^{*}[k-\Delta] e^{-j2\pi\alpha k}. \tag{27}$$

Given that a total of N_{c} samples of $Y_{\text{DT}}[n]$ were received, then we consider n in the range $0 \leq n \leq N_{\text{c}} - 1$, and the autocorrelated CAF is evaluated as [12, Eqn. (13)], [13, Eqn. (13)] (we set $Y_{\text{DT}}[n] = 0$ for $n < 0$ or $n \geq N_{\text{c}}$):

$$\overline{\mathcal{R}}_{Y_{\text{DT}}}[\alpha, \Delta; N_{\text{lag}}] = \frac{1}{N_{\text{c}}} \sum_{n=N_{\text{lag}}}^{N_{\text{c}}-N_{\text{seg}}} \mathcal{R}_{Y_{\text{DT}}}^{\alpha}[n, \Delta]_{N_{\text{seg}}} \cdot \left(\mathcal{R}_{Y_{\text{DT}}}^{\alpha}[n - N_{\text{lag}}, \Delta]_{N_{\text{seg}}}\right)^{*} \tag{28}$$

From [12, Sec. III-A], [13, Secs. 3.1, 3.3] it follows that the optimal value of the lag parameter N_{lag}, which guarantees that the cycle frequencies are unambiguously obtained from the autocorrelated CAF, is equal to N_{seg}. Using this assignment, and summing over the lag variable $\Delta \in \mathcal{N}_\Delta$, we obtain the cost function [13, Eqn. (24)]

$$\mathcal{C}_{Y_{\text{DT}}}(\alpha) = \sum_{\Delta\in\mathcal{N}_\Delta} \overline{\mathcal{R}}_{Y_{\text{DT}}}[\alpha, \Delta; N_{\text{seg}}]. \tag{29}$$

In [12, Appendix], [13, Sec. 3.2] it is shown that for sufficiently large values of N_{c}, the autocorrelated CAF (28) approaches the expression (assuming synchronized sampling)

$$\overline{\mathcal{R}}_{Y_{\text{DT}}}[\alpha, \Delta; N_{\text{seg}}] \approx \sum_{\alpha_Y\in\mathcal{A}_{\text{wscs}}} \left|\mathcal{R}_{Y_{\text{DT}}}^{\alpha_Y}[\Delta]\right|^2 \delta(\alpha - \alpha_Y) \cdot e^{j2\pi(\alpha-\alpha_Y)N_{\text{seg}}}$$

and the cost function (29) approaches

$$\mathcal{C}_{Y_{\text{DT}}}(\alpha) \approx \sum_{\alpha_Y\in\mathcal{A}_{\text{wscs}}} \sum_{\Delta\in\mathcal{N}_\Delta} \left|\mathcal{R}_{Y_{\text{DT}}}^{\alpha_Y}[\Delta]\right|^2 \delta(\alpha - \alpha_Y) \cdot e^{j2\pi(\alpha-\alpha_Y)N_{\text{seg}}} \tag{30}$$

It can be observed from (30) that the peaks of $\mathcal{C}_{Y_{\text{DT}}}(\alpha)$ occur at the cycle frequencies of the set $\mathcal{A}_{\text{wscs}}$. For asynchronous sampling Eqn. (30) holds with the countable set of cycle frequencies $\mathcal{A}_{\text{wsacs}}$ is used instead of the finite set $\mathcal{A}_{\text{wscs}}$. Hence, an efficient algorithm for acquisition of the cycle frequencies can be implemented by searching for the peaks of the cost function $\mathcal{C}_{Y_{\text{DT}}}(\alpha)$. Considering a maximal value of α denoted by $\alpha_{N_{\text{T}}}$, then for the range $\mathcal{A} \triangleq (0, \alpha_{N_{\text{T}}}]$, an efficient estimate of the cycle frequencies of $Y_{\text{DT}}[n]$, denoted $\hat{\mathcal{A}}_{\text{DT}}$, can be implemented by identifying the local maxima of $\mathcal{C}_{Y_{\text{DT}}}(\alpha)$ considering only values above a threshold amplitude level C_{TH}, e.g.,

$$\hat{\mathcal{A}}_{\text{DT}} = \left\{\alpha \in \mathcal{A} \middle| \{\mathcal{C}_{Y_{\text{DT}}}(\alpha) > C_{\text{TH}}\} \cap \{\alpha \text{ is a local maxima}\}\right\} \tag{31}$$

In the rest of this paper we denote the parameters corresponding to a non-synchronized sampling rate using the superscript (ns), e.g., $T_{\text{samp}}^{(\text{ns})} \neq T_{\text{samp}}^{(\text{sync})}$ denotes the non-synchronized sampling interval.

A. EVALUATING THE COST FUNCTION FOR $f_{samp}^{(ns)} > f_{samp}^{(sync)}$ AND FOR $f_{samp}^{(ns)} < f_{samp}^{(sync)}$

We next illustrate the relationship between the cost function and the sampling frequency offset. To that aim we consider the following scenario:

Consider a transmitted sequence of M OFDM symbols where each OFDM symbol comprises of $N_{\text{sym}} = N_{\text{sc}} + N_{\text{cp}}$ samples. The total number of samples in the transmitted sequence is therefore $N_{\text{c}} = M \cdot N_{\text{sym}}$. We consider a slowly varying frequency selective fading channel such that the channel remains constant over the transmission of M subsequent OFDM symbols [17], [19]. Assuming L paths between the transmitter and the receiver, the CIR can be written as

$$h(t) = \sum_{l=0}^{L-1} a_l \cdot \delta(t - \tau_l), \tag{32}$$

where a_l and τ_l represent, respectively, the path gain and path delay corresponding to path l. In the numerical evaluations, unless stated otherwise, we use a multipath delay profile with $L = 6$ different paths specified in Table 1. In each frame, $M = 20$ OFDM symbols are transmitted with $N_{\text{sc}} = 128$ and $N_{\text{cp}} = 32$, hence, $N_{\text{sym}} = 160$.

Let the synchronized sampling rate be $f_{\text{samp}}^{(\text{sync})} = \frac{1}{T_{\text{samp}}^{(\text{sync})}} = 4$ MHz [22]. Fig. 2 depicts the cost functions $\mathcal{C}_{Y_{\text{DT}}}^{(\text{sync})}(\alpha)$ and $\mathcal{C}_{Y_{\text{DT}}}^{(\text{ns})}(\alpha)$ for sampling rates $f_{\text{samp}}^{(\text{sync})}$ and $f_{\text{samp}}^{(\text{ns})} = 0.7 \cdot f_{\text{samp}}^{(\text{sync})}$, respectively, with $M = 20$, $N_{\text{seg}} = 2^8$, and $E_b/N_0 = 5$ dB. As the peaks along the cycle frequency axis correspond to the

TABLE 1. Multipath delay profile.

Path #	Complex gain	Relative delay (samples)
1	$1.05-0.82i$	0
2	$0.71+0.45i$	4
3	$0.63-0.72i$	9
4	$0.53+0.62i$	13
5	$0.41+0.37i$	17
6	$0.20-0.34i$	21

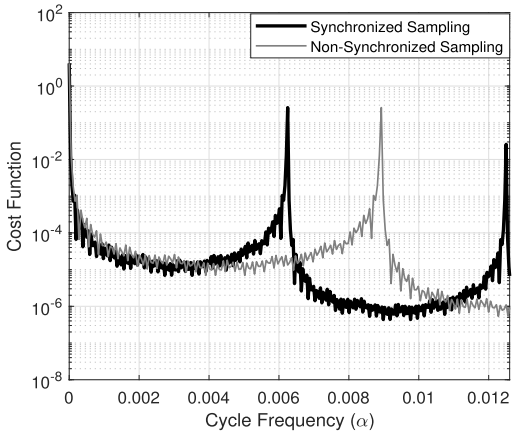

FIGURE 2. The cost functions $C_{Y_{\mathrm{DT}}}^{(\mathrm{sync})}(\alpha)$ and $C_{Y_{\mathrm{DT}}}^{(\mathrm{ns})}(\alpha)$ (refer Eqn. (29)) for sampling rates $f_{\mathrm{samp}}^{(\mathrm{sync})}$ and $f_{\mathrm{samp}}^{(\mathrm{ns})}=0.7\cdot f_{\mathrm{samp}}^{(\mathrm{sync})}$, respectively.

values of the cycle frequencies (see (30)), then with $N_{\mathrm{T}}=2$, the estimated cycle frequencies from $C_{Y_{\mathrm{DT}}}^{(\mathrm{ns})}(\alpha)$ in the range $\mathcal{A}=(0,\alpha_2]=(0,0.0125]$ consist of a single cycle frequency $\hat{\alpha}_1^{(\mathrm{ns})}=0.00892$. Recall that the stationary AWGN does not exhibit cyclostationarity, hence, it does not affect the non-zero cycle frequencies. We observe that when $f_{\mathrm{samp}}^{(\mathrm{ns})}<f_{\mathrm{samp}}^{(\mathrm{sync})}$, the cycle frequencies are distanced further apart in the axis of cycle frequencies than for the original signal.

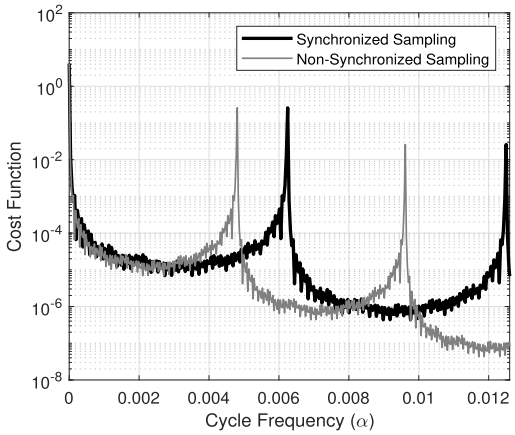

FIGURE 3. The cost functions $C_{Y_{\mathrm{DT}}}^{(\mathrm{sync})}(\alpha)$ and $C_{Y_{\mathrm{DT}}}^{(\mathrm{ns})}(\alpha)$ (refer Eqn. (29)) for sampling rates $f_{\mathrm{samp}}^{(\mathrm{sync})}$ and $f_{\mathrm{samp}}^{(\mathrm{ns})}=1.3\cdot f_{\mathrm{samp}}^{(\mathrm{sync})}$, respectively.

Fig. 3 depicts the cost functions $C_{Y_{\mathrm{DT}}}^{(\mathrm{sync})}(\alpha)$ and $C_{Y_{\mathrm{DT}}}^{(\mathrm{ns})}(\alpha)$ for the sampling rate $f_{\mathrm{samp}}^{(\mathrm{sync})}$ and $f_{\mathrm{samp}}^{(\mathrm{ns})}=1.3\cdot f_{\mathrm{samp}}^{(\mathrm{sync})}$, respectively, with $M=20$, $N_{\mathrm{seg}}=2^8$, and $E_b/N_0=5$ dB. With $N_{\mathrm{T}}=2$, the estimated cycle frequencies based on $C_{Y_{\mathrm{DT}}}^{(\mathrm{ns})}(\alpha)$ in the range $\mathcal{A}=(0,\alpha_2]=(0,0.0125]$ are $\hat{\alpha}_1=0.00480$, and $\hat{\alpha}_2$=0.00961. It is observed that for $f_{\mathrm{samp}}^{(\mathrm{ns})}>f_{\mathrm{samp}}^{(\mathrm{sync})}$ the cycle frequencies are closer in the axis of cycle frequencies than for the original signal.

Remark 1: As explained in [12, Sec. III], [13, Sec. 3.1] the resolution of the cycle frequencies estimation is $\frac{1}{N_{\mathrm{seg}}}$, hence, as N_{seg} increases, the resolution and accuracy of the CAF estimation via (27) improves, which improves the accuracy of the cycle frequencies estimation scheme based on (29). On the other hand, it directly follows from Table 2 that the computational complexity increases linearly as N_{seg} increases. It thus follows that the value of N_{seg} is selected as a compromise between these two opposite effects, and that it is generally preferred to use the minimal N_{seg} which facilitates the required estimation accuracy, see [13, Sec. 3.3]. In the numerical evaluations reported in the manuscript we used $N_{\mathrm{sym}}=160$, hence, the fundamental cycle frequency of the transmitted signal is $\frac{1}{160}=0.00625$. The smallest observed fundamental cycle frequency is obtained for the largest considered SFO, which in our evaluations corresponds to $\overline{f}_{\mathrm{samp}}^{(\mathrm{ns})}=1.3$. For this SFO, the fundamental cycle frequency of the received DT signal is $\frac{1}{1.3}0.00625=0.0048$. Therefore, the smallest positive integer P such that $\frac{1}{2^P}<0.0048$ is 8: $2^{-8}\approx 0.0039$, hence, $N_{\mathrm{seg}}=256$ is the minimal N_{seg} which provides the required resolution. Lastly, we note that N_{seg} is restricted to be a power of 2 in order facilitate the application of the FFT in the evaluation of Eqn. (27), leading to a more computationally efficient implementation, see also [13, Sec. 3.3].

B. SEQUENTIAL STEPS OF THE CB-SFS ALGORITHM

The observations in Figs. 2 and 3 facilitate the motivation for the robust blind CB-SFS algorithm we present in this subsection for estimating $T_{\mathrm{samp}}^{(\mathrm{sync})}$. We first note that as practically ξ is very small, then the cycle frequencies of the WSACS process are nearly equidistant, hence, the WSACS process can be (nearly) regarded as a WSCS process for the practical purpose of SFO estimation, as we apply in the proposed algorithm. We further note that while previous SFO estimation algorithms assumed a perfect symbol time offset synchronization at the receiver (see, e.g., [17]), the proposed estimator assumes that the receiver is not synchronized with respect to the OFDM symbol time, which is a more practically relevant scenario for SFO estimation in wireless communications systems. To overcome the lack of symbol time offset synchronization, the receiver uses an extended observation window of length $N_{\mathrm{sym}}\cdot(M+1)$ samples as depicted in Fig. 4.

We next detail the steps of the CB-SFS algorithm:

1) PARAMETER INITIALIZATION

The receiver initially obtains the following parameters:

- $\alpha_{N_{\mathrm{T}}}$: The cycle frequency corresponding to the N_{T}-th peak of the cost function (29) in the range $\mathcal{A}=(0,\alpha_{N_{\mathrm{T}}}]$

TABLE 2. Computational complexity of the cb-sfs method (a detailed derivation is provided in appendix B).

Step	Description	Term	CA	CM
1.	Compute segmented CAF	$\mathcal{R}^{\alpha}_{Y_{\rm DT}}[n,\Delta]_{N_{\rm seg}}$	$(2N_{\rm c}-3N_{\rm seg}-1)\lvert\mathcal{N}_\Delta\rvert N_{\rm seg}$	$2(N_{\rm c}-N_{\rm seg})\lvert\mathcal{N}_\Delta\rvert N_{\rm seg}$
2.	Evaluate autocorrelated CAF	$\overline{\mathcal{R}}_{Y_{\rm DT}}[\alpha,\Delta;N_{\rm seg}]$	$\big(N_{\rm c}-2N_{\rm seg}\big)\lvert\mathcal{N}_\Delta\rvert N_{\rm seg}$	$\big(N_{\rm c}-2N_{\rm seg}+1\big)\lvert\mathcal{N}_\Delta\rvert N_{\rm seg}$
3.	Evaluate the cost function	$\mathcal{C}_{Y_{\rm DT}}(\alpha)$	$(\lvert\mathcal{N}_\Delta\rvert-1)N_{\rm seg}$	
	Total Complexity		$\big(\lvert\mathcal{N}_\Delta\rvert(3N_{\rm c}-5N_{\rm seg})-1\big)N_{\rm seg}$	$\big(3N_{\rm c}-4N_{\rm seg}+1\big)\lvert\mathcal{N}_\Delta\rvert N_{\rm seg}$

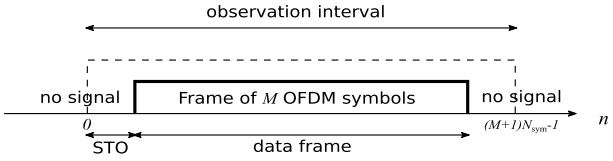

FIGURE 4. Extending the observation interval to accommodate lack of STO synchronization.

for synchronized sampling. This parameter is uniquely determined by the OFDM symbol length $N_{\rm sym}$, hence, using its a-priori knowledge of $N_{\rm sym}$, the receiver knows the cycle frequencies for synchronous sampling, which are given by $\alpha_k \triangleq \frac{k}{N_{\rm sym}}; 0 \le k \le N_{\rm T}$, and sets $\alpha_{N_{\rm T}} = \frac{N_{\rm T}}{N_{\rm sym}}$.

- $T^{(\rm ns)}_{\rm samp}$: The current sampling interval at the receiver.
- M : The total number of OFDM symbols used for SFO estimation.
- $N_{\rm seg}$: The segment length used for the evaluation of the cost function (29).

2) ALGORITHM STEPS

Using the measurements $\{Y_{\rm DT}[n]\}_{n=0}^{N_{\rm c}-1}$, the CB-SFS algorithm now proceeds with the following steps:

1) Evaluate the segmented CAF of $Y_{\rm DT}[n]$, $\mathcal{R}^{\alpha}_{Y_{\rm DT}}[n,\Delta]_{N_{\rm seg}}$ via (27).
2) Evaluate the autocorrelated CAF $\overline{\mathcal{R}}_{Y_{\rm DT}}[\alpha,\Delta;N_{\rm lag}]$ via (28), using the segmented CAF with $N_{\rm lag} = N_{\rm seg}$, as suggested in [12, Sec. III-A], [13, Secs. 3.1, 3.3].
3) Compute the cost function $\mathcal{C}^{(\rm ns)}_{Y_{\rm DT}}(\alpha)$ via (29) for the values of $\alpha \in \big\{\frac{i}{N_{\rm seg}}\alpha_{N_{\rm T}}; i=1,2,\cdots,N_{\rm seg}\big\}$.
4) Estimate the cycle frequencies in the range $\mathcal{A} = (0,\alpha_{N_{\rm T}}]$. Let the highest cycle frequency identified by the receiver in this range be denoted by $\hat{\alpha}^{(\rm ns)}_{N_{\rm last}}$, and the peak count corresponding to that cycle frequency be the $N_{\rm last}$-th peak. Let $\alpha^{(\rm ns)}_1$ be the fundamental cycle frequency for the non-synchronously sampled signal $Y_{\rm DT}[n]$. Since for DT cyclostationary processes, the cycle frequencies are integer multiples of the fundamental cycle frequency, the fundamental cycle frequency can be estimated as
$$\hat{\alpha}^{(\rm ns)}_1 = \frac{\hat{\alpha}^{(\rm ns)}_{N_{\rm last}}}{N_{\rm last}}. \tag{33}$$
5) Lastly, the synchronized sampling interval is estimated as
$$\hat{T}^{(\rm sync)}_{\rm samp} = \left(\frac{\alpha_1}{\hat{\alpha}^{(\rm ns)}_1}\right) T^{(\rm ns)}_{\rm samp}. \tag{34}$$

Remark 2: The cycle frequency offset between the fundamental frequencies is obtained as
$$\widehat{\Delta\alpha_1} = \hat{\alpha}^{(\rm ns)}_1 - \alpha_1$$
Note that when $\widehat{\Delta\alpha_1} > 0$, then $T^{(\rm ns)}_{\rm samp} > T^{(\rm sync)}_{\rm samp}$ while when $\widehat{\Delta\alpha_1} < 0$, then $T^{(\rm ns)}_{\rm samp} < T^{(\rm sync)}_{\rm samp}$.

C. COMPLEXITY OF THE CB-SFS ALGORITHM

Table 2 details the computational complexity of the proposed CB-SFS algorithm in terms of complex multiplications (CMs) and complex additions (CAs), where the complexities of computing the different quantities used in the algorithm are stated in Table 2 as well. In the table, $|\mathcal{N}_\Delta|$ represents the total number of lag values for which the correlation is non-zero for at least one time instant within a period. Note that the cycle frequencies are estimated using a grid search in the parameter α. In the numerical evaluations we implement this search using $N_{\rm seg}$ points, and this value is used in the complexity expressions in Table 2.

VI. NUMERICAL RESULTS AND DISCUSSIONS

The numerical evaluations use the OFDM signal parameters detailed in Section III, namely, for each OFDM symbol, $N_{\rm sc} = 128$ and $N_{\rm cp} = 32$, hence, $N_{\rm sym} = 160$.

A. DEMONSTRATION OF THE CB-SFS ALGORITHM

In the following we illustrate the computations of the steps of the proposed CB-SFS algorithm for a specific test scenario.

Initialization:

- $N_{\rm T} = 2$, thus $\mathcal{A} = (0, 0.0125]$.
- $T^{(\rm ns)}_{\rm samp} = T^{(\rm sync)}_{\rm samp}/\sqrt{2}$, $M = 20$, $N_{\rm seg} = 2^8$.

The computations in the steps of the CB-SFS algorithm are as follows:

Steps $1-3$: In steps 1-3, the cost function of (29) is computed for the received signal obtained by sampling at $T^{(\rm ns)}_{\rm samp}$, denoted $\mathcal{C}^{(\rm ns)}_{Y_{\rm DT}}(\alpha)$, for $E_b/N_0 = 10$ dB and a channel whose CIR is $h(t) = \delta(t)$. Fig. 5 depicts $\mathcal{C}^{(\rm ns)}_{Y_{\rm DT}}(\alpha)$ for $\alpha \in \mathcal{A}$. In Fig. 5 we also include the cost function for the synchronized sampling interval $T^{(\rm sync)}_{\rm samp}$, denoted $\mathcal{C}^{(\rm sync)}_{Y_{\rm DT}}(\alpha)$, only for the purpose of highlighting the operation of the algorithm. It is emphasized that $\mathcal{C}^{(\rm sync)}_{Y_{\rm DT}}(\alpha)$ *is not required for the estimation process*. It can be observed from the figure that the SFO results in an offset between the cycle frequencies of the signal obtained with non-synchronized sampling relative to those of the signal obtained with synchronized sampling.

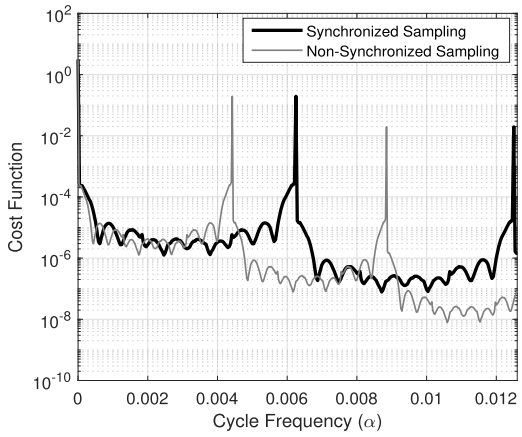

FIGURE 5. The cost function (refer Eqn. (29)) for the sampling intervals $T_{\text{samp}}^{(\text{sync})}$ and $T_{\text{samp}}^{(\text{ns})}$.

Next, steps 4 and 5 are computed as follows:

4) For non-synchronized sampling interval $T_{\text{samp}}^{(\text{ns})}$, using the cost function $\mathcal{C}_{Y_{\text{DT}}}^{(\text{ns})}(\alpha)$, we obtain the cycle frequency $\hat{\alpha}_{N_{\text{last}}}^{(\text{ns})}$, which corresponds to the N_{last}-th peak in the range $\mathcal{A}$, as $\hat{\alpha}_{N_{\text{last}}}^{(\text{ns})} = \hat{\alpha}_2^{(\text{ns})} = 0.008848$. The fundamental cycle frequency for the non-synchronized sampling can be obtained as

$$\hat{\alpha}_1^{(\text{ns})} = \frac{\hat{\alpha}_{N_{\text{last}}}^{(\text{ns})}}{N_{\text{last}}} = \frac{0.008848}{2} = 0.004424.$$

Note that the cycle frequency offset for the fundamental cycle frequency can be obtained as

$$\widehat{\Delta\alpha_1} = \hat{\alpha}_1^{(\text{ns})} - \alpha_1 = -0.001826,$$

which is in agreement with Remark 2.

5) The synchronized sampling interval $T_{\text{samp}}^{(\text{sync})}$ can be estimated as

$$\hat{T}_{\text{samp}}^{(\text{sync})} = \left(\frac{\alpha_1}{\hat{\alpha}_1^{(\text{ns})}}\right) T_{\text{samp}}^{(\text{ns})} = 0.25\mu\text{sec}$$

The SFO can be estimated using the estimate $\hat{T}_{\text{samp}}^{(\text{sync})}$ as

$$\hat{\eta} = \frac{T_{\text{samp}}^{(\text{ns})} - \hat{T}_{\text{samp}}^{(\text{sync})}}{\hat{T}_{\text{samp}}^{(\text{sync})}} = -0.29289.$$

Note that the exact SFO can be computed from the relationship $T_{\text{samp}}^{(\text{ns})} = T_{\text{samp}}^{(\text{sync})}/\sqrt{2}$ as:

$$\eta = \frac{T_{\text{samp}}^{(\text{ns})} - T_{\text{samp}}^{(\text{sync})}}{T_{\text{samp}}^{(\text{sync})}} = -0.2928932.$$

It can be observed that the proposed CB-SFS algorithm yields an accurate estimate $\hat{\eta}$ of the SFO η.

B. PERFORMANCE COMPARISON WITH PREVIOUS WORKS

We evaluated the performance of the proposed CB-SFS algorithm in estimating SFOs in the range of $f_{\text{samp}}^{(\text{ns})} = 0.7 \cdot f_{\text{samp}}^{(\text{sync})}$ to $f_{\text{samp}}^{(\text{ns})} = 1.3 \cdot f_{\text{samp}}^{(\text{sync})}$. Therefore, the normalized sampling frequency $\overline{f}_{\text{samp}}^{(\text{ns})} \triangleq f_{\text{samp}}^{(\text{ns})}/f_{\text{samp}}^{(\text{sync})}$ ranges from 0.7 to 1.3. In the following, comparisons are made with three previously proposed algorithms: The first is the DA ML algorithm proposed in [8, Algorithm 1]. Here, two time domain observations containing the repetitive training sequences are used for computing the correlation, followed by interpolation and zero padding. Subsequently, a grid search is applied to obtain the estimated SFO. The second previously proposed algorithm is the SFO estimation scheme proposed in [5], which estimates the SFO using cyclic delay diversity (CDD), based on the pilot carriers having maximum channel powers. We note that while CDD is designed for MISO channels, we assume that the estimator can achieve periodicity of the channel in the current setup - which is an assumption which favors CDD. The third previously proposed algorithm is the scheme proposed in [7] which estimates the SFO via an efficient LSE based on continual pilots. In the ML, CDD and the LSE algorithms, BPSK modulation is used for the pilot symbols where the CDD algorithm and the LSE algorithm are each implemented with $N_{\text{p}}^{(\text{LSE})}$=$N_{\text{p}}^{(\text{CDD})} = 14$ pilots. In this context, it is emphasized that the proposed CB-SFS algorithm does not require the use of pilot symbols for SFO estimation thereby avoiding the associated decrease in spectral efficiency. We note that the LSE and the CDD schemes use the channel coefficients in computing the estimated SFO. Thus, when considering the practical application of these schemes, these coefficients have to be estimated. In the simulations reported in this section we use the exact channel coefficients for these algorithms, hence CDD's and LSE's performance in the simulations are lower bounds on their actual performance. An important aspect in the application of the CB-SFS algorithm is that as the CB-SFS algorithm uses the periodicity of the statistics to determine the SFO, then in order to facilitate its application, it needs to observe a minimal number of OFDM symbols, *irrespective of the number of subcarriers per OFDM symbol*. Based on preliminary numerical tests we obtain that it is sufficient to use 13 OFDM symbols to obtain the full performance of the CB-SFS algorithm. This is mainly due to the need to facilitate cycle frequency estimation for asynchronous sampling, giving rise to WSACS statistics of the received signal. Accordingly, the numerical evaluations use the signal parameters detailed at the beginning of Section VI, where in each frame $M = 13$ OFDM symbols are transmitted. The channel model used is detailed in Section III, namely, the channel is modeled as a multipath channel with a multipath delay profile consisting of $L = 6$ different paths, whose coefficients are specified in Table 1. We note that for the specified OFDM parameters, with $f_{\text{samp}}^{(\text{sync})} = \frac{1}{T_{\text{samp}}^{(\text{sync})}} = 4$ MHz [22], this corresponds to an overall duration of 0.52 msec which implies that the CB-SFS algorithm is applicable also to time-varying channels (note that the typical coherence time for wireless channels in the frequency range of 700-2400 MHz is 5-10 msec [23], [24]). Each simulation point was evaluated with 10^5 experiments. In the following, comparisons will be made w.r.t.

E_b/N_0, see, e.g., [22], [25], to facilitate a fair comparison with different modulations. Lastly, we note that while [10] and [11] proposed blind SFO estimation algorithms, we did not include them in the numerical study as their performance were inferior to those of the CDD and LSE algorithms as can be observed in [10, Sec. IV] and [11, Sec. IV].

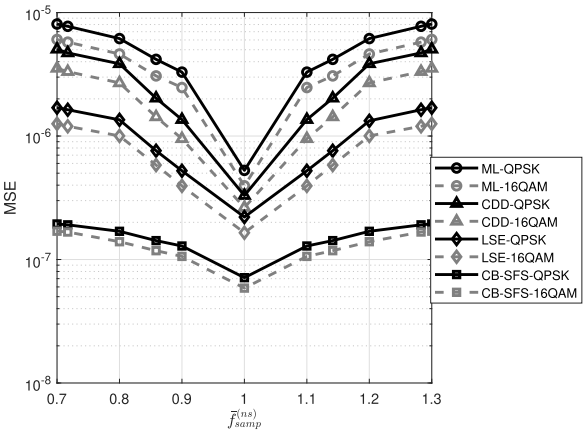

FIGURE 6. MSE vs. $\bar{f}^{(ns)}_{samp}$ for the ML, the CDD, the LSE and the CB-SFS algorithms corresponding to different modulation formats for E_b/N_0=−5 dB with the multipath channel specified in Table 1.

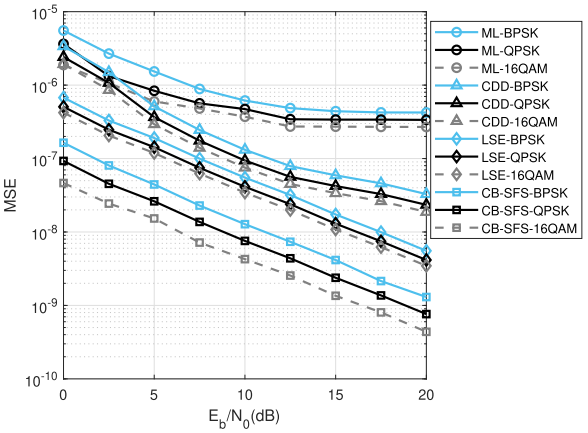

FIGURE 7. MSE vs. E_b/N_0 for the ML, the CDD, the LSE and the CB-SFS algorithms corresponding to different modulation formats with $\bar{f}^{(ns)}_{samp}=1-0.2\cdot\sqrt{2}\approx 0.71$ and the multipath channel specified in Table 1.

Fig. 6 depicts the mean-squared error (MSE) performance for SFO estimation, normalized to $f^{(sync)}_{samp}$, for the ML algorithm, the CDD algorithm, the LSE algorithm and the proposed CB-SFS algorithm vs. $\bar{f}^{(ns)}_{samp}$, for $E_b/N_0 = -5$ dB. Here, the ML, CDD, LSE and CB-SFS algorithms are set to be symbol synchronized, i.e., operate with perfect STO synchronization. Superiority and robustness of the CB-SFS algorithm, compared to the CDD, LSE and ML algorithms is evident. Fig. 7 depicts the MSE performance of the ML algorithm, the CDD algorithm, the LSE algorithm and the CB-SFS algorithm vs. E_b/N_0 for the *asynchronous sampling frequency* of $\bar{f}^{(ns)}_{samp}=1-0.2\cdot\sqrt{2}\approx 0.71$, where perfect STO

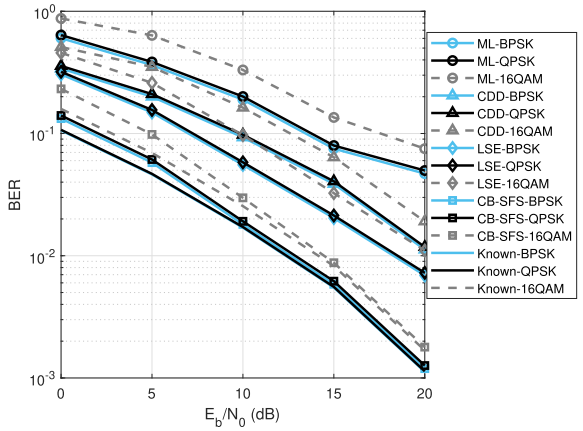

FIGURE 8. BER vs. E_b/N_0 for the ML, the CDD, the LSE and the CB-SFS algorithms corresponding to different modulation formats with $\bar{f}^{(ns)}_{samp}=1-0.2\cdot\sqrt{2}\approx 0.71$ and the multipath channel specified in Table 1.

synchronization is considered at the receiver. The CB-SFS algorithm, the LSE and the CDD algorithms show improvement in the MSE with an increase in E_b/N_0 whereas the ML algorithm attains an error floor.

We note that as the key performance parameter for communications systems is the BER at the receiver, it is important to understand how the BER is affected by the MSE of the SFO estimation. In this context, we note that as SFO results in loss of orthogonality between subcarriers, then a larger SFO directly leads to a higher BER, and thus it follows that a larger MSE in SFO estimation results in a higher BER. To demonstrate this relationship, we repeated the simulations corresponding to Fig. 7, but this time depicting the uncoded BER instead of the MSE for 16QAM, QPSK and BPSK, vs. E_b/N_0, for $\bar{f}^{(ns)}_{samp} = 1-0.2\cdot\sqrt{2}\approx 0.71$. The results are depicted in Fig. 8. Comparing with Fig. 7, a direct proportional relationship between the MSE and the uncoded BER is clearly observed. It is also observed that for QPSK and BPSK, the uncoded BER with CB-SFS *practically coincides* with the uncoded BER obtained with *ideal* SFO correction. This further demonstrates the superiority of CB-SFS over the baseline schemes. Lastly, we note that a similar relationship between uncoded BER and MSE in SFO estimation can be observed in [5, Figs. 1, 2, 4] which depict the MSE and the uncoded BER for the CDD algorithm vs. SNR.

Next, Fig. 9 presents the normalized MSE performance of the ML algorithm, the CDD algorithm, the LSE algorithm and the CB-SFS algorithm for $\bar{f}^{(ns)}_{samp}= 1-0.2\cdot\sqrt{2}\approx 0.71$ and $E_b/N_0 = -5$ dB, at STO values of 4, 7, 11 and 15 samples w.r.t. sequence start time. The CB-SFS algorithm uses an extended observation interval of $(M+1)\cdot N_{sym}$ instead of $M\cdot N_{sym}$ to account for the STO. It is observed that both the CB-SFS and the CDD algorithms demonstrate robustness to STO synchronization errors, while STO effect is more pronounced for the LSE and the ML algorithms. The robustness of the CDD algorithm follows as the signal design facilitates SFO estimation in which the impact of STO is significantly reduced by averaging, while for the LSE and

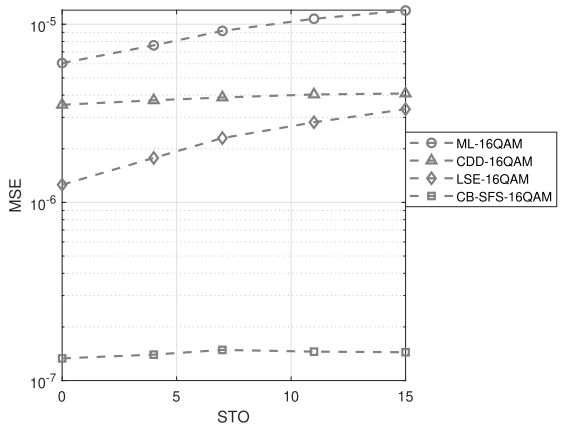

FIGURE 9. MSE vs. STO for the ML, the CDD, the LSE and the CB-SFS algorithms for 16QAM modulation with $\bar{f}_{\text{samp}}^{(\text{ns})}=1-0.2\cdot\sqrt{2}\approx 0.71$ at $E_b/N_0=-5$ dB over the multipath channel specified in Table 1.

for the ML algorithms, the received signal model used for designing the estimator does not account for STO, resulting in the STO having a significant effect on the phase component which is used for the estimation of the SFO. Recall that the superior performance of the CF-SFS algorithm, observed in Figs. 6, 7, and 9, are obtained using a short synchronization sequence, which comprises of only 13 OFDM symbols, with an overall time duration of 0.52 msec (assuming $f_{\text{samp}}^{(\text{sync})}=\frac{1}{T_{\text{samp}}^{(\text{sync})}}=4\,\text{MHz}$ [22]). This clearly indicates that the CB-SFS algorithm is suitable for SFO synchronization also over time-varying channels.

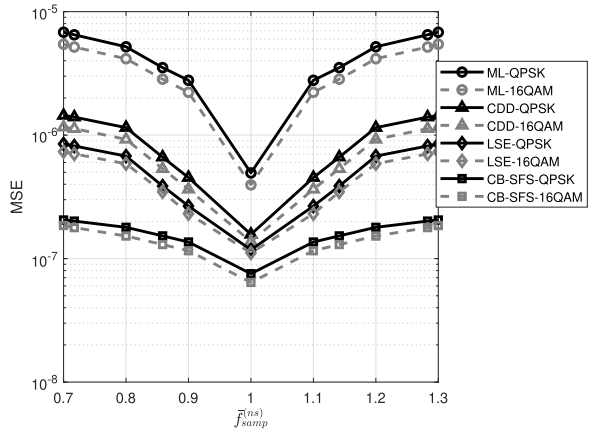

FIGURE 10. MSE vs. $\bar{f}_{\text{samp}}^{(\text{ns})}$ for the ML, the CDD, the LSE and the CB-SFS algorithms corresponding to different modulation formats for $E_b/N_0=-5$ dB with the multipath channel specified in Table 1. LSE and CDD use additional pilots to approach the performance of CB-SFS.

In order to demonstrate the tradeoff between performance and spectral efficiency, we increased the number of pilots in the LSE and the CDD algorithms such that their MSE performances approach that of the CB-SFS. To that aim, we used $N_p^{(\text{LSE})}=22$ and $N_p^{(\text{CDD})}=26$ pilots. For this setup, Fig. 10 depicts the MSE performance evaluated at normalized sampling frequency $\bar{f}_{\text{samp}}^{(\text{ns})}$ and $E_b/N_0=-5$ dB, subject to perfect STO synchronization at the receiver. It can be noted from the figure that indeed, using more pilots has improved the performance of the LSE and of the CDD algorithms, which are now quite close to that of the CB-SFS algorithm, at the expense of decreasing the spectral efficiency (computed as the ratio of the number of subcarriers used for data transmission to the total number of subcarriers of the OFDM symbol, N_{sc}): The spectral efficiencies of the LSE algorithm and of the CDD algorithm are now lower than that of the CB-SFS algorithm by 18% and 21% respectively. This loss in spectral efficiency is a critical consideration in design of practical systems.

C. COMPARISON OF COMPUTATIONAL COMPLEXITY AND REQUIRED A-PRIORI KNOWLEDGE

The numerical evaluations show that the CB-SFS algorithm, which does not require a pilot sequence, achieves excellent performance at a high spectral efficiency as all subcarriers are used for data transmission. Specifically, considering the scenario in Fig. 10 where MSE performance of CDD and LSE are quite close to that of CB-SFS, we observe that the spectral efficiency of the CB-SFS algorithm is 18%-21% higher than that of the CDD and LSE algorithms. In order to present the complete picture we must also address the computational complexity cost of this performance advantage. Table 3 details the computational complexity of the algorithms compared above in terms of their CMs and CAs *per grid search point*. For LSE, as no grid search is used, the overall computational complexity is included. Table 3 also includes the spectral efficiency for the parameters of Fig. 10

In the following discussion, we compare the computational complexity of the different algorithms via their order of CMs, as multiplications dominate the computational complexity. Using the parameters for which the plots in Fig. 10 were generated, for evaluating the CM computational complexity via the expressions in Table 3, we obtain that the CB-SFS algorithm has a CM complexity per grid search point on the order of $\mathcal{O}\left(1.440\cdot 10^3\cdot M\right)$, and the CM complexity of the ML algorithm and of the CDD algorithm per grid search point is on the order of $\mathcal{O}\left(16.384\cdot 10^3\cdot M\right)$ and $\mathcal{O}\left(0.416\cdot 10^3\cdot M\right)$, respectively. As the LSE algorithm does not employ a grid search, then for maintaining fairness of comparison we normalize its total CM complexity expression from Table 3 by the size of the grid used in the numerical evaluations, which is $N_{\text{seg}}=2^8$. This results in a normalized CM complexity for the LSE on the order of $\mathcal{O}\left(2.112\cdot 10^3/256\cdot M\right)=\mathcal{O}\left(0.00825\cdot 10^3\cdot M\right)$. It follows that the computational complexity of the new CB-SFS algorithm is lower than that of the ML algorithm but somewhat higher than that of the CDD and the LSE algorithms, yet, similarly to ML, LSE and CDD, the complexity of CB-SFS is linear in the length of the sequence, M. At the same time, CB-SFS offers much higher spectral efficiency for the same performance as well as high robustness to channel CIR, due to blindness of the scheme, as well as to STO synchronization errors.

TABLE 3. Computational complexity of the estimation schemes (per grid search point).

Estimator	CA	CA Order	CM	CM Order	Spectral Efficiency (Fig. 10)
CB-SFS algorithm	$\lvert\mathcal{N}_\Delta\rvert(3N_c - 5N_{seg}) - 1$	$\mathcal{O}(3\lvert\mathcal{N}_\Delta\rvert MN_{sym})$	$(3N_c - 4N_{seg} + 1)\lvert\mathcal{N}_\Delta\rvert$	$\mathcal{O}(3\lvert\mathcal{N}_\Delta\rvert MN_{sym})$	1
ML algorithm [8]	$MN_{sc}^2 + N_{sc}\log_2 N_{sc}$	$\mathcal{O}(MN_{sc}^2)$	$4MN_{sc}^2 + N_{sc}(N_{sc}+1)$	$\mathcal{O}(4MN_{sc}^2)$	0.9
CDD algorithm [5]	$10MN_p^{(CDD)} - 12$	$\mathcal{O}(10MN_p^{(CDD)})$	$16MN_p^{(CDD)} - 2$	$\mathcal{O}(16MN_p^{(CDD)})$	0.796875
LSE algorithm* [7]	$6N_p^{(LSE)}(8M-7) - 1$	$\mathcal{O}(48MN_p^{(LSE)})$	$12N_p^{(LSE)}(8M-7) - 1$	$\mathcal{O}(96MN_p^{(LSE)})$	0.828125

* As the LSE algorithm does not implement a grid search, its total complexity is stated.

In terms of the required a-priori knowledge, the proposed CB-SFS algorithm requires only the knowledge of the cycle frequency threshold parameter α_{N_T} for estimating the cycle frequencies. This parameter directly follows from the value of N_{sym}, which is a system parameter. The ML algorithm in [8, Algorithm 1] requires knowledge of the predefined pilot sequence. Similarly, the LSE algorithm of [7] requires knowledge of the dedicated continual pilot symbols, and the CDD algorithm of [5] requires knowledge of the suitable cyclic delay and predefined pilot symbols, which are used for sampling frequency synchronization. As both LSE and CDD use the channel coefficients in the computation of the estimates, then, for time-varying channels, it should be noted that the channel has to be estimated using a relatively small number of observations. This will necessarily lead to unreliable estimates, which, in turn, will further degrade the performance of these schemes compared to their performance depicted in the simulations using the exact channel coefficients.

VII. CONCLUSIONS

In this paper, a computationally and spectrally efficient blind algorithm for sampling frequency synchronization is proposed. The algorithm first estimates the cycle frequencies of the DT received signal and then determines the sampling frequency offset as the offset required to align the cycle frequencies of the DT received signal with those of the DT transmitted signal, which are a-priori known at the receiver. To the best of our knowledge, this is the first instance of an SFO estimation algorithm based on the DT received signal which does not require knowledge of the channel and does not use pilots or non-linearities. The numerical simulations show that the proposed CB-SFS algorithm yields excellent estimation performance for a wide range of sampling frequency offsets, and exhibits robustness to channel multipath. Moreover, the analysis shows that the proposed algorithm is computationally feasible when compared with the existing estimators.

APPENDIX A
CYCLOSTATIONARITY OF $R(t)$

Using the statistics of $D_{m,k}$ in (10) and the expressions for $R(t)$ in (14), the AF of $R(t)$ can be derived as (35), as shown at the top of the next page. Next, from (10) it follows that $\mathbb{E}\{(D_{m,k})^2\} = 0$, hence the expression for $\mathcal{R}_R(t,\tau)$ in (35) specializes to (36), as shown at the top of the next page. Letting $\underline{m} = (m-1)$, then, as m varies from $-\infty$ to ∞, it follows that $\underline{m}$ varies from $-\infty$ to ∞ as well. Hence, the expression for $\mathcal{R}_R(t+T_{sym},\tau)$ can be obtained from Eqn. (36) as in Eqn. (37), as shown at the top of the next page. It follows from the Eqns. (36) and (37) that $\mathcal{R}_R(t,\tau) = \mathcal{R}_R(t+T_{sym},\tau)$. Hence, combined with (18) it follows that $R(t)$ is a WSCS process.

APPENDIX B
COMPUTATIONAL COMPLEXITY OF THE CB-SFS ALGORITHM

As discussed earlier in the Sec. V, the optimal value of the lag parameter N_{lag}, which guarantees that the cycle frequencies are unambiguously obtained from the autocorrelated CAF, is equal to N_{seg}. The computational complexity of the CB-SFS algorithm follows from the first three steps. This complexity is derived in the following.

Step 1 (Computing the segmented CAF for the entire computation): The segmented CAF of $Y_{DT}[n]$ in (27) is expressed as:

$$\mathcal{R}^{\alpha}_{Y_{DT}}[n,\Delta]_{N_{seg}} = \frac{1}{N_{seg}}\sum_{k=n}^{n+N_{seg}-1} Y_{DT}[k]\cdot Y^*_{DT}[k-\Delta]\cdot e^{-j2\pi\alpha k}$$

Note that $Y_{DT}[k]$ is obtained for $0 \le k \le N_c - 1$. Now, when n in (27) equals $n = N_{seg}$ we have:

$$\mathcal{R}^{\alpha}_{Y_{DT}}[N_{seg},\Delta]_{N_{seg}} = \frac{1}{N_{seg}}\sum_{k=N_{seg}}^{2N_{seg}-1} Y_{DT}[k]\cdot Y^*_{DT}[k-\Delta]\cdot e^{-j2\pi\alpha k}$$

where the number of CAs is $N_{seg}-1$ and the number of CMs is $2N_{seg}$.

For evaluating the total number of CAs, note that the remaining values of n vary from $N_{seg}+1$ upto $N_c - N_{seg}$, see (28), where for each index n, $\mathcal{R}^{\alpha}_{Y_{DT}}[n,\Delta]_{N_{seg}}$ can be obtained from $\mathcal{R}^{\alpha}_{Y_{DT}}[n-1,\Delta]_{N_{seg}}$ with one addition (of $Y_{DT}[n+N_{seg}-1]\cdot Y^*_{DT}[n+N_{seg}-1-\Delta]\cdot e^{-j2\pi\alpha(n+N_{seg}-1)}$) and one subtraction (of $Y_{DT}[n-1]\cdot Y^*_{DT}[n-1-\Delta]\cdot e^{-j2\pi\alpha(n-1)}$). The total number of corresponding CAs is thus $2\big((N_c - N_{seg}) - (N_{seg}+1)+1\big) = 2(N_c - 2N_{seg})$. Adding the number of CAs for the initial computation of $\mathcal{R}^{\alpha}_{Y_{DT}}[N_{seg},\Delta]_{N_{seg}}$, which is $N_{seg}-1$, it follows that the total number of CAs is $2(N_c - 2N_{seg}) + (N_{seg}-1) = 2N_c - 3N_{seg} - 1$. Using N_{seg} resolution points for α in the range $(0,\alpha_{N_T}]$ and accounting for the $\lvert\mathcal{N}_\Delta\rvert$ lag values with non-zero correlation, we obtain that the total number of CAs for the computation of all the values

$$\mathcal{R}_R(t,\tau) \triangleq \mathbb{E}\{R(t)R^*(t-\tau)\}$$
$$= \frac{1}{4\,T_{\rm sc}} \sum_{m=-\infty}^{\infty} \sum_{k=0}^{N_{\rm sc}-1} \Bigg[\Bigg(\sigma_D^2 e^{j2\pi\left(\Delta_{\rm f}+\frac{k}{T_{\rm sc}}\right)\tau} \int_{\lambda=0}^{\infty} h(\lambda) e^{-j2\pi\left(f_{\rm Tx}+\frac{k}{T_{\rm sc}}\right)\lambda} p(t-\lambda-mT_{\rm sym})d\lambda \int_{\tilde{\lambda}=0}^{\infty} h(\tilde{\lambda}) e^{j2\pi\left(f_{\rm Tx}+\frac{k}{T_{\rm sc}}\right)\tilde{\lambda}}$$
$$\cdot p(t-\tau-\tilde{\lambda}-mT_{\rm sym})d\tilde{\lambda} \Bigg) + \Bigg(\mathbb{E}\{(D_{m,k})^2\} e^{j4\pi f_{\rm Tx}t} e^{j2\phi_{\rm Tx}} e^{-j2\pi\left(\Sigma_{\rm f}+\frac{k}{T_{\rm sc}}\right)\tau} e^{j4\pi\frac{k}{T_{\rm sc}}(t-mT_{\rm sym})}$$
$$\cdot \int_{\lambda=0}^{\infty} h(\lambda) e^{-j2\pi\left(f_{\rm Tx}+\frac{k}{T_{\rm sc}}\right)\lambda} p(t-\lambda-mT_{\rm sym})d\lambda \int_{\tilde{\lambda}=0}^{\infty} h(\tilde{\lambda}) e^{-j2\pi\left(f_{\rm Tx}+\frac{k}{T_{\rm sc}}\right)\tilde{\lambda}} p(t-\tau-\tilde{\lambda}-mT_{\rm sym})d\tilde{\lambda} \Bigg)$$
$$+ \Bigg(\mathbb{E}\{(D_{m,k}^*)^2\} e^{-j4\pi f_{\rm Tx}t} e^{-j2\phi_{\rm Tx}} e^{j2\pi\left(\Delta_{\rm f}+\frac{k}{T_{\rm sc}}\right)\tau} e^{-j4\pi\frac{k}{T_{\rm sc}}(t-mT_{\rm sym})} \int_{\lambda=0}^{\infty} h(\lambda) e^{-j2\pi\left(f_{\rm Tx}+\frac{k}{T_{\rm sc}}\right)\lambda} p(t-\lambda-mT_{\rm sym})d\lambda$$
$$\cdot \int_{\tilde{\lambda}=0}^{\infty} h(\tilde{\lambda}) e^{-j2\pi\left(f_{\rm Tx}+\frac{k}{T_{\rm sc}}\right)\tilde{\lambda}} p(t-\tau-\tilde{\lambda}-mT_{\rm sym})d\tilde{\lambda} \Bigg) + \Bigg(\sigma_D^2 e^{-j2\pi\left(\Sigma_{\rm f}+\frac{k}{T_{\rm sc}}\right)\tau} \int_{\lambda=0}^{\infty} h(\lambda) e^{j2\pi\left(f_{\rm Tx}+\frac{k}{T_{\rm sc}}\right)\lambda}$$
$$\cdot p(t-\lambda-mT_{\rm sym})d\lambda \int_{\tilde{\lambda}=0}^{\infty} h(\tilde{\lambda}) e^{-j2\pi\left(f_{\rm Tx}+\frac{k}{T_{\rm sc}}\right)\tilde{\lambda}} p(t-\tau-\tilde{\lambda}-mT_{\rm sym})d\tilde{\lambda} \Bigg) \Bigg] + \mathcal{R}_W(\tau) \tag{35}$$

$$\mathcal{R}_R(t,\tau) = \frac{1}{4\,T_{\rm sc}} \sum_{m=-\infty}^{\infty} \sum_{k=0}^{N_{\rm sc}-1} \Bigg[\Bigg(\sigma_D^2\, e^{j2\pi\left(\Delta_{\rm f}+\frac{k}{T_{\rm sc}}\right)\tau} \int_{\lambda=0}^{\infty} h(\lambda) e^{-j2\pi\left(f_{\rm Tx}+\frac{k}{T_{\rm sc}}\right)\lambda} p(t-\lambda-mT_{\rm sym})d\lambda$$
$$\cdot \int_{\tilde{\lambda}=0}^{\infty} h(\tilde{\lambda}) e^{j2\pi\left(f_{\rm Tx}+\frac{k}{T_{\rm sc}}\right)\tilde{\lambda}} p(t-\tau-\tilde{\lambda}-mT_{\rm sym})d\tilde{\lambda} \Bigg) + \Bigg(\sigma_D^2\, e^{-j2\pi\left(\Sigma_{\rm f}+\frac{k}{T_{\rm sc}}\right)\tau} \int_{\lambda=0}^{\infty} h(\lambda) e^{j2\pi\left(f_{\rm Tx}+\frac{k}{T_{\rm sc}}\right)\lambda}$$
$$\cdot p(t-\lambda-mT_{\rm sym})d\lambda \int_{\tilde{\lambda}=0}^{\infty} h(\tilde{\lambda}) e^{-j2\pi\left(f_{\rm Tx}+\frac{k}{T_{\rm sc}}\right)\tilde{\lambda}}\, p(t-\tau-\tilde{\lambda}-mT_{\rm sym})d\tilde{\lambda} \Bigg) \Bigg] + \mathcal{R}_W(\tau) \tag{36}$$

$$\mathcal{R}_R(t+T_{\rm sym},\tau) = \frac{1}{4\,T_{\rm sc}} \sum_{\underline{m}=-\infty}^{\infty} \sum_{k=0}^{N_{\rm sc}-1} \Bigg[\Bigg(\sigma_D^2\, e^{j2\pi\left(\Delta_{\rm f}+\frac{k}{T_{\rm sc}}\right)\tau} \int_{\lambda=0}^{\infty} h(\lambda) e^{-j2\pi\left(f_{\rm Tx}+\frac{k}{T_{\rm sc}}\right)\lambda}\, p(t-\lambda-\underline{m}T_{\rm sym})d\lambda$$
$$\cdot \int_{\tilde{\lambda}=0}^{\infty} h(\tilde{\lambda}) e^{j2\pi\left(f_{\rm Tx}+\frac{k}{T_{\rm sc}}\right)\tilde{\lambda}} p(t-\tau-\tilde{\lambda}-\underline{m}T_{\rm sym})d\tilde{\lambda} \Bigg) + \Bigg(\sigma_D^2\, e^{-j2\pi\left(\Sigma_{f}+\frac{k}{T_{\rm sc}}\right)\tau} \int_{\lambda=0}^{\infty} h(\lambda) e^{j2\pi\left(f_{\rm Tx}+\frac{k}{T_{\rm sc}}\right)\lambda}$$
$$\cdot p(t-\lambda-\underline{m}T_{\rm sym})d\lambda \int_{\tilde{\lambda}=0}^{\infty} h(\tilde{\lambda}) e^{-j2\pi\left(f_{\rm Tx}+\frac{k}{T_{\rm sc}}\right)\tilde{\lambda}} p(t-\tau-\tilde{\lambda}-\underline{m}T_{\rm sym})d\tilde{\lambda} \Bigg) \Bigg] + \mathcal{R}_W(\tau) \tag{37}$$

of the segmented CAF used in the estimation of the cycle frequencies is $(2N_{\rm c}-3N_{\rm seg}-1)|\mathcal{N}_\Delta|N_{\rm seg}$.

For evaluating the total number of CMs, again note that beyond $k = N_{\rm seg}$, we have that the value of k varies from $N_{\rm seg}+1$ up to $N_{\rm c}-N_{\rm seg}$ (see (28)), where each new value is associated with 2 multiplications. Therefore, the total number of CMs beyond the first evaluation (corresponding to $k = N_{\rm seg}$) is $2\big((N_{\rm c}-N_{\rm seg})-(N_{\rm seg}+1)+1\big) = 2(N_{\rm c}-2N_{\rm seg})$. Adding the $2N_{\rm seg}$ multiplications from the initial calculation results in a total number of CMs of $2(N_{\rm c}-2N_{\rm seg})+2N_{\rm seg} = 2(N_{\rm c}-N_{\rm seg})$. Accounting for the $N_{\rm seg}$ resolution points for α and for the $|\mathcal{N}_\Delta|$ lag values with non-zero correlation, it follows that the total number of CMs for evaluating all the required values of the segmented CAF is $2(N_{\rm c}-N_{\rm seg})|\mathcal{N}_\Delta|N_{\rm seg}$.

Step 2 (Computing the autocorrelated CAF for the entire computation): Using (28), the autocorrelated CAF (with $N_{\rm lag}=N_{\rm seg}$) is evaluated as:

$$\overline{\mathcal{R}}_{Y_{\rm DT}}[\alpha,\Delta;N_{\rm seg}] = \frac{1}{N_{\rm c}} \sum_{n=N_{\rm seg}}^{N_{\rm c}-N_{\rm seg}} \mathcal{R}^{\alpha}_{Y_{\rm DT}}[n,\Delta]_{N_{\rm seg}} \cdot \Big(\mathcal{R}^{\alpha}_{Y_{\rm DT}}[n-N_{\rm seg},\Delta]_{N_{\rm seg}}\Big)^*$$

It is observed that the total number of CAs required for evaluating all values of the autocorrelated CAF required for cycle frequencies estimation is $(N_{\rm c}-2N_{\rm seg})\,|\mathcal{N}_\Delta|N_{\rm seg}$ and the total number of CMs is $(N_{\rm c}-2N_{\rm seg}+1)\,|\mathcal{N}_\Delta|N_{\rm seg}$.

Step 3 (Evaluating the cost function): The cost function is presented in Eqn. (29) as:

$$\mathcal{C}_{Y_{\rm DT}}(\alpha) = \sum_{\Delta\in\mathcal{N}_\Delta} \overline{\mathcal{R}}_{Y_{\rm DT}}[\alpha,\Delta;N_{\rm seg}].$$

The total number of CAs for evaluating the cost function at all resolution points is thus $(|\mathcal{N}_\Delta|-1)N_{\rm seg}$.

REFERENCES

[1] H. Bogucka, P. Kryszkiewicz, and A. Kliks, "Dynamic spectrum aggregation for future 5G communications," *IEEE Commun. Mag.*, vol. 53, no. 5, pp. 35–43, May 2015.

[2] R. V. Nee and R. Prasad, *OFDM for Wireless Multimedia Communications*. Norwood, MA, USA: Artech House, 2000.

[3] M. Speth, S. Fechtel, G. Fock, and H. Meyr, "Optimum receiver design for OFDM-based broadband transmission. II. A case study," *IEEE Trans. Commun.*, vol. 49, no. 4, pp. 571–578, Apr. 2001.

[4] Y.-H. You and K.-T. Lee, "Accurate pilot-aided sampling frequency offset estimation scheme for DRM broadcasting systems," *IEEE Trans. Broadcast.*, vol. 56, no. 4, pp. 558–563, Dec. 2010.

[5] Y.-H. You, Y.-A. Jung, and J.-H. Paik, "Joint estimation of symbol timing and sampling frequency offset for CDD-OFDM-based DRM systems," *IEEE Trans. Broadcast.*, vol. 65, no. 2, pp. 333–339, Jun. 2019.
[6] Y.-H. Kim and J.-H. Lee, "Joint maximum likelihood estimation of carrier and sampling frequency offsets for OFDM systems," *IEEE Trans. Broadcast.*, vol. 57, no. 2, pp. 277–283, Jun. 2011.
[7] Y.-A. Jung, J.-Y. Kim, and Y.-H. You, "Complexity efficient least squares estimation of frequency offsets for DVB-C2 OFDM systems," *IEEE Access*, vol. 6, pp. 35165–35170, 2018.
[8] J. Yuan and M. Torlak, "Joint CFO and SFO estimator for OFDM receiver using common reference frequency," *IEEE Trans. Broadcast.*, vol. 62, no. 1, pp. 141–149, Mar. 2016.
[9] B. Chen and H. Wang, "Blind estimation of OFDM carrier frequency offset via oversampling," *IEEE Trans. Signal Process.*, vol. 52, no. 7, pp. 2047–2057, Jul. 2004.
[10] X. Li, J. Hu, W. Heng, F. Yu, and G. Wang, "Blind carrier and sampling frequency offsets estimation in OFDM system," in *Proc. WCNC*, San Francisco, CA, USA, Mar. 2017, pp. 1–6.
[11] A. Laourine, A. Stephenne, and S. Affes, "Blind sampling clock offset estimation in OFDM systems based on second order statistics," in *Proc. 40th Asilomar Conf. Signals, Syst. Comput.*, Pacific Grove, CA, USA, Oct. 2006, pp. 1782–1785.
[12] G. K. Yeung and W. A. Gardner, "Search-efficient methods of detection of cyclostationary signals," *IEEE Trans. Signal Process.*, vol. 44, no. 5, pp. 1214–1223, May 1996.
[13] Y. Hu, B. Yu, Z. Deng, G. He, and H. Zhou, "Efficient cycle frequency acquisition of a cyclostationary signal with the FACA method," *Radioengineering*, vol. 28, no. 2, pp. 447–455, Jun. 2019.
[14] W. A. Gardner, A. Napolitano, and L. Paura, "Cyclostationarity: Half a century of research," *Signal Process.*, vol. 86, no. 4, pp. 639–697, 2006.
[15] H. Bohr, *Almost Periodic Functions*. New York, NY, USA: Courier Dover Publications, 2018.
[16] A. Napolitano, "Cyclostationarity: Limits and generalizations," *Signal Process.*, vol. 120, pp. 323–347, Mar. 2016.
[17] Y. Murin and R. Dabora, "Low complexity estimation of carrier and sampling frequency offsets in burst-mode OFDM systems," *Wireless Commun. Mobile Comput.*, vol. 16, no. 9, pp. 1018–1034, Jun. 2016.
[18] N. Shlezinger and R. Dabora, "Frequency-shift filtering for OFDM signal recovery in narrowband power line communications," *IEEE Trans. Commun.*, vol. 62, no. 4, pp. 1283–1295, Apr. 2014.
[19] W.-L. Chin, "ML estimation of timing and frequency offsets using distinctive correlation characteristics of OFDM signals over dispersive fading channels," *IEEE Trans. Veh. Technol.*, vol. 60, no. 2, pp. 444–456, Feb. 2011.
[20] L. Izzo and A. Napolitano, "Higher-order cyclostationarity properties of sampled time-series," *Signal Process.*, vol. 54, no. 3, pp. 303–307, Nov. 1996.
[21] N. Shlezinger, K. Todros, and R. Dabora, "Adaptive filtering based on time-averaged MSE for cyclostationary signals," *IEEE Trans. Commun.*, vol. 65, no. 4, pp. 1746–1761, Apr. 2017.
[22] H.-G. Jeon, K.-S. Kim, and E. Serpedin, "An efficient blind deterministic frequency offset estimator for OFDM systems," *IEEE Trans. Commun.*, vol. 59, no. 4, pp. 1133–1141, Apr. 2011.
[23] *LTE: Evolved Universal Terrestrial Radio Access (E-UTRA) Use Equipment (UE) Radio Transmission and Reception*, document 3GPP TS 36.101, Ver. 10.30, 2011.
[24] *Guidelines for Evaluation of Radio Transmission Technologies for IMT-2000*, Int. Telecommun. Union (ITU), Geneva, CH, document M.1225, 1997.
[25] M. Morelli and M. Moretti, "Fine carrier and sampling frequency synchronization in OFDM systems," *IEEE Trans. Wireless Commun.*, vol. 9, no. 4, pp. 1514–1524, Apr. 2010.

MANISH KUMAR received the Ph.D. degree in electrical engineering from IIT Patna, India, in 2018. He is currently a Researcher with the Department of Electrical and Computer Engineering, Ben-Gurion University, Israel. His current research interests include signal detection and estimation theory, cyclostationary signal processing, OFDM and its receiver synchronization, MIMO communications, and cognitive radio networks.

RON DABORA received the B.Sc. and M.Sc. degrees in electrical engineering from Tel-Aviv University, in 1994 and 2000, respectively, and the Ph.D. degree from Cornell University, in 2007. From 1994 to 2000, he was with the Ministry of Defense of Israel. From 2000 to 2003, he was with the Algorithms Group, Millimetrix Broadband Networks Ltd., Israel, and from 2007 to 2009, he was a Postdoctoral Researcher with the Department of Electrical Engineering, Stanford University. Since 2009, he has been with the Department of Electrical and Computer Engineering, Ben-Gurion University, Israel, where he is currently an Associate Professor. His research interests include network information theory, wireless communications, and power line communications. He served as a TPC Member of a number of international conferences, including WCNC, PIMRC, and ICC. From 2012 to 2014, he was an Associate Editor of the IEEE Signal Processing Letters. He was a Senior Area Editor of the IEEE Signal Processing Letters, from 2014 to 2019.